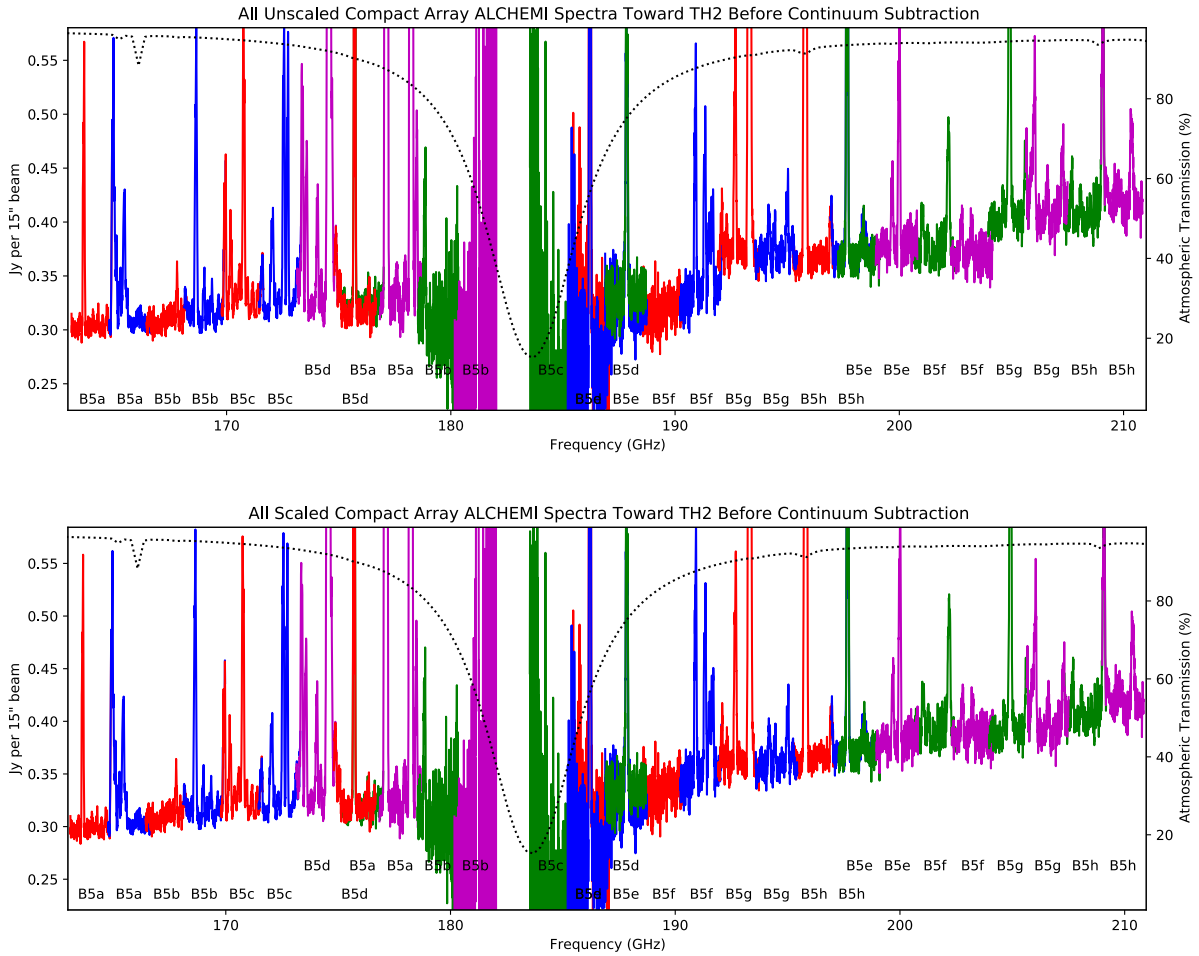


**Fig. B.4.** Same as Fig. B.2 but for Band 5 unscaled (top) and scaled (bottom).

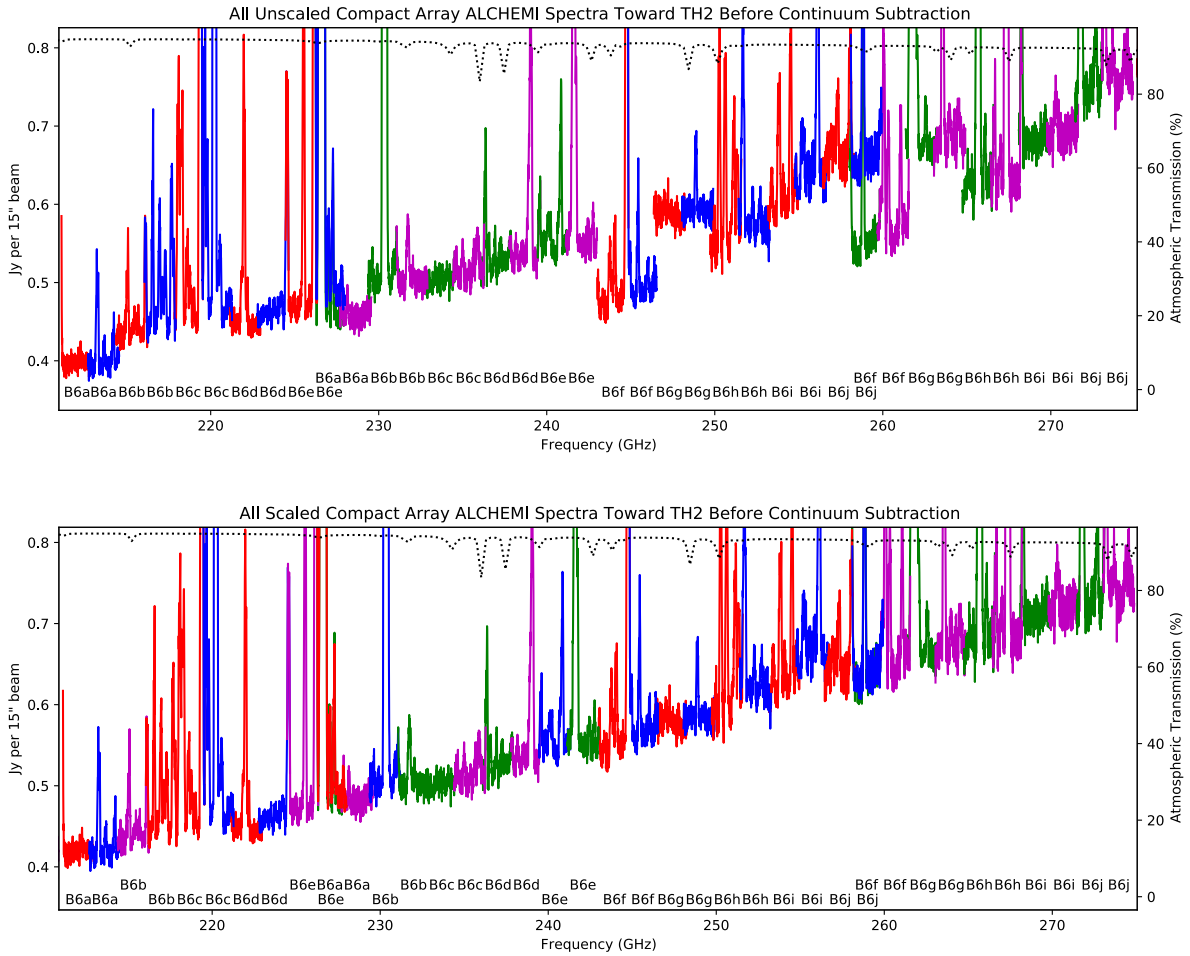


**Fig. B.5.** Same as Fig. B.2 but for Band 6 unscaled (top) and scaled (bottom).

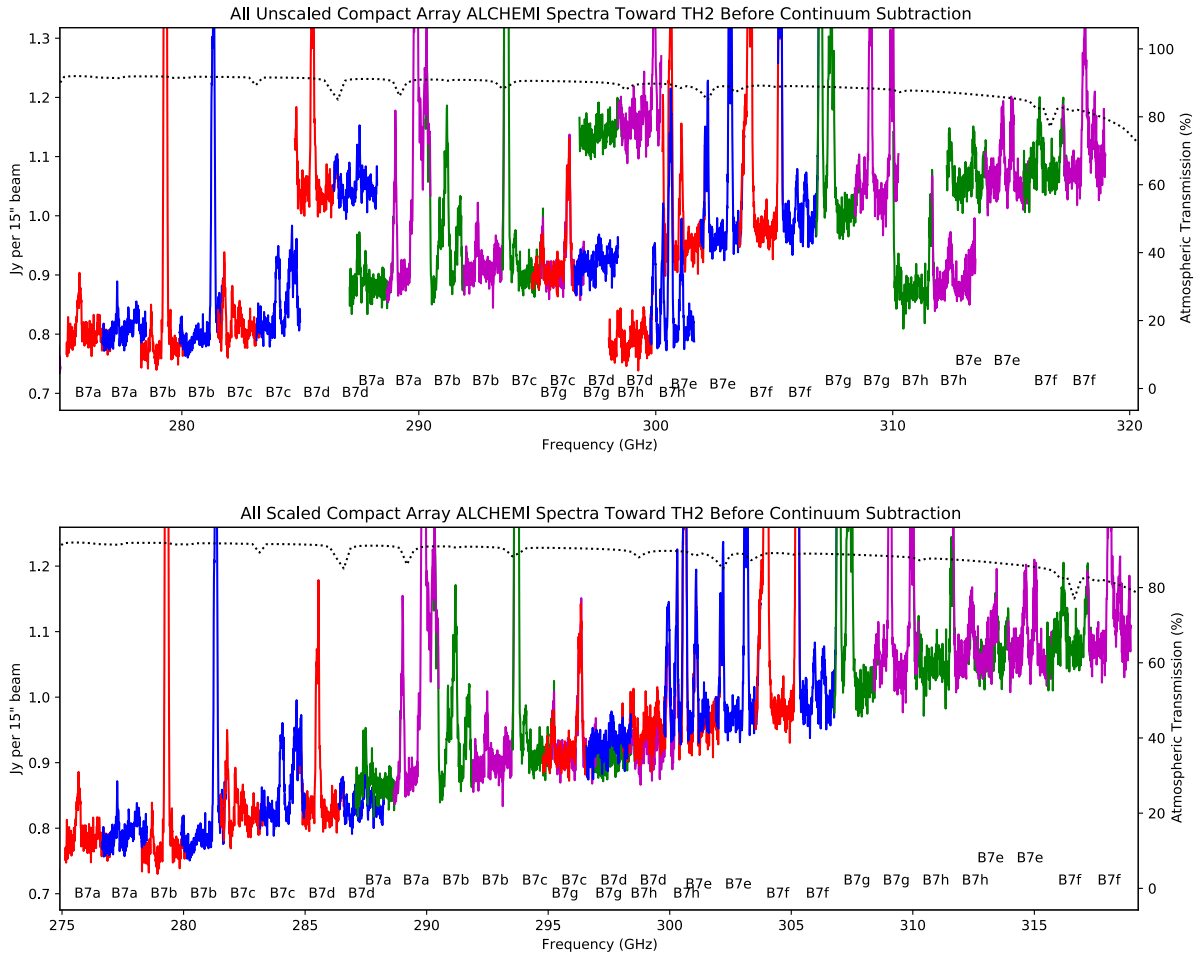


**Fig. B.6.** Same as Fig. B.2 but for the first-half of Band 7 unscaled (top) and scaled (bottom).

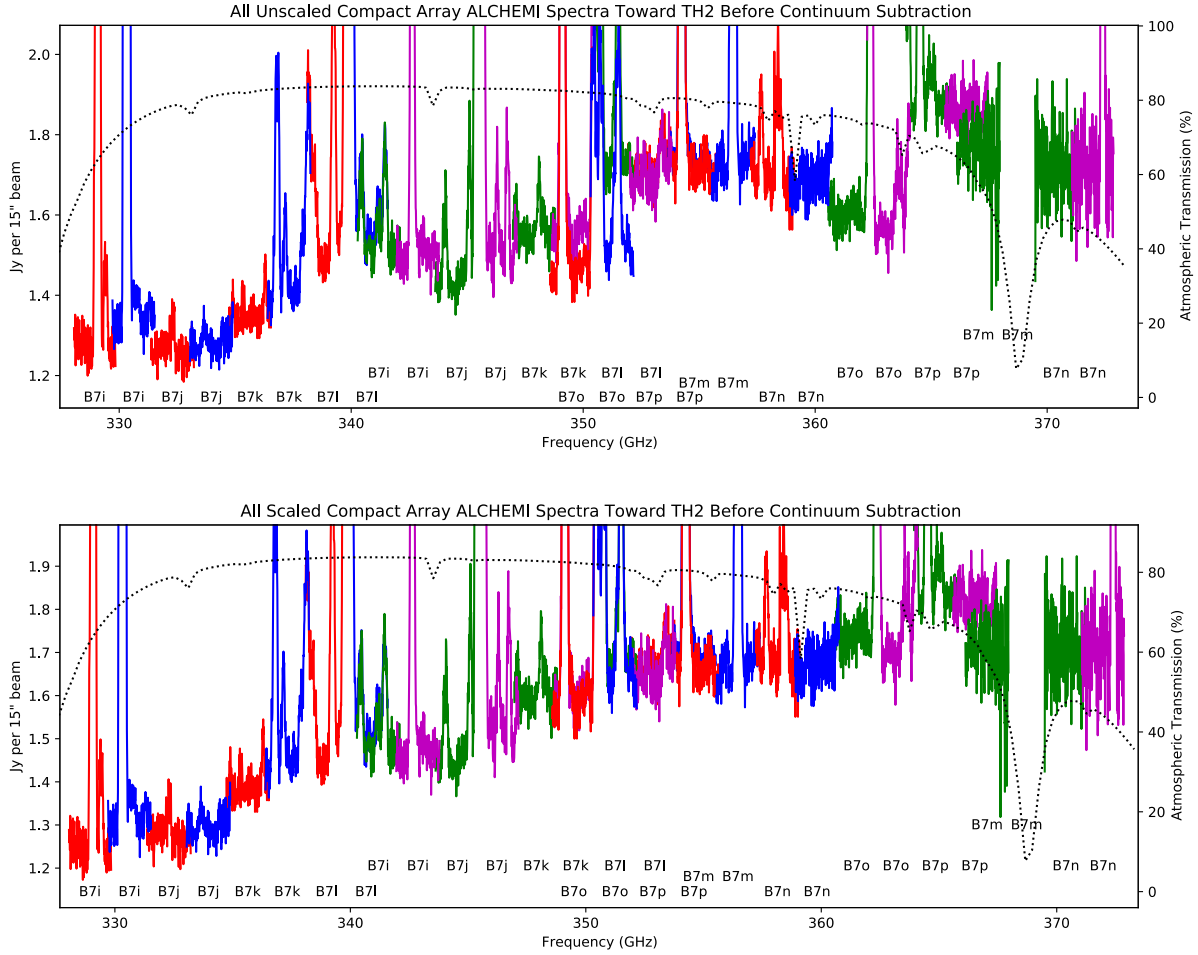


**Fig. B.7.** Same as Fig. B.2 but for the second half of Band 7 unscaled (top) and scaled (bottom).

## Appendix C: ALCHEMI Flux Calibration

The ALMA flux calibration process includes a number of contributions to its uncertainty, including systematic errors within a given measurement calibrated with a single primary flux reference such as that due to:

1. The primary flux calibrator model used to set the absolute flux calibration scale.
2. The primary flux calibrator measurement used to define the reference point for the secondary flux calibrator flux.

as well as random uncertainties due to:

1. The bootstrapping from the primary to the secondary flux calibrator.
2. The bootstrapping from the secondary flux calibrator to the target source.
3. The lack of a proper elevation-dependent opacity correction during any of the bootstrapping steps.

Furthermore, even though extra mitigation measures can be done during an observation to account for items 4 and 5 above, there is nothing that can allow one to attain an absolute flux calibration error that is better than the error associated with the primary flux calibrator measurement and model.

Early in the process of imaging the ALCHEMI measurements, amplitude offsets between overlapping receiver tunings were noted (see Sect. 3.1 and Appendix B). The analysis of these offsets has given ALCHEMI the ability to correct for "at least one component" of the flux calibration uncertainty. This flux calibration alignment, though, does not allow for the determination of the absolute flux calibration reference. At best we have corrected the flux scales within our individual scheduling blocks to a common value. The ALCHEMI image cubes have been corrected for these flux rescaling factors, which we believe has corrected for noise introduced as part of the flux calibration process after the primary flux calibrator measurement.

In the following we address two levels of flux calibration uncertainty in the ALCHEMI data: Relative flux calibration, which represents the flux calibration uncertainty to be used when comparing fluxes within the ALCHEMI image cubes for a given set of imaging inputs (i.e., array, spatial, and spectral resolution); Absolute flux calibration, which represents the flux calibration uncertainty to be used when comparing fluxes derived from the ALCHEMI image cubes for comparison with other (non-ALCHEMI) measurements.

### C.1. Relative Flux Calibration Uncertainty

The spectral flux normalization that we have applied to all ALCHEMI measurement sets has effectively normalized all ALCHEMI data to a common flux calibration scale for each array configuration[5] measured in the ALCHEMI survey. This implies that we have normalized all ALCHEMI data measured with a given array configuration to the same relative flux calibration scale. This furthermore implies that comparison of spectral lines within the ALCHEMI survey can be compared using a relative flux calibration uncertainty.

The statistics of the amplitude scaling factors given in Table A.1 are provided in Table C.1. It is noteworthy that for our Band 3 measurements the 12mE configuration shows significant deviations from the average values of the scaling factors for that receiver band and configuration.

An estimate of the relative flux calibration uncertainty associated with a given receiver band and configuration can be derived from the scatter in the scaling factors (Table C.1) that we have applied to our measurement sets to normalize them to the same mean flux scale. The RMS values for the flux scale normalization factors for each Band and array configuration(s) (listed as Compact Array / Extended Array / Combined) are:

- Band 3: 2% / 12% / 12%
- Band 4: 1% / 2% / 2%
- Band 5: 2% / 2% / 2%
- Band 6: 5% / 1% / 5%
- Band 7: 8% / 3% / 9%

The relative flux calibration uncertainty for the ALCHEMI image cubes which are combinations of the Compact Array and Extended Array measurements will in reality be a complex combination of the relative flux calibration uncertainties, which itself depends upon the contribution of each array measurement to a given flux in the ALCHEMI survey. The contribution of each array to the combined measurement is dependent upon numerous factors such as relative visibility contributions and time-dependent variations between the individual array measurements. In the above, we conservatively estimate the relative flux calibration uncertainty for the combined values as the root-sum-square of the Compact Array and Extended Array scaling factor RMS values.

Be aware that the actual "flux uncertainty" to be used in a line-ratio analysis, for example, is not determined solely by the "flux calibration uncertainty" in complex sources such as NGC 253. The line flux one measures depends on how the imaging process (robust parameter, clean mask, clean depth, selfcal, *etc.*) has been performed and on the properties of the spectral line itself. The same imaging parameters can have different effects on different spectral lines. For example, when different spectral lines have distinct spatial extents or when one spectral line is bright and the other is faint because the brighter spectral line has a larger fraction of its flux cleaned. For these reasons, the real flux calibration uncertainty is likely to be larger than that assumed from an assessment of the quality of the flux calibration process alone.

### C.2. Absolute Flux Calibration Uncertainty

The absolute flux calibration uncertainty starts with the relative flux calibration uncertainty and includes contributions due to the measurement, model, and application of the primary flux calibration source (see above). To estimate this additional contribution, we assume that the measurement of the relatively bright sources used as primary flux calibrators provide a negligible contribution to the primary flux calibration uncertainty. This uncertainty is then dominated by that associated with the primary flux calibrator model. Models used by ALMA within CASA are unlikely to be accurate to <5% (Butler 2012, priv. comm.). We use then the following recommendations for flux calibration accuracy, from the ALMA Proposer's Guide for Cycle 5[2] (Section A.9.2 on "Flux Accuracy"), as an estimate of the primary flux calibrator model uncertainty:

- Bands 3, 4, 5: < 5%
- Bands 6, 7, 8: < 10%
- Bands 9 and 10: < 20%

The absolute flux calibration uncertainty, including the relative flux calibration uncertainty derived for the ALCHEMI image cubes, is given by the root-sum-squared of the relative

[5] By array configuration we mean to differentiate among the Compact Array, either ACA (7m) or 12m Compact (12mC), the Extended Array (12m/12mE) and Combined (12m7m/12mE12mC) that were used for each spectral setup. Each of these observations consisted of a number of individual observations with slightly varying array configurations depending on the antenna availability at the time of the observation.

**Table C.1.** Statistics by bands and arrays of the relative flux scaling factors ($a_i$)

| Band | Array | $N_{obs}$[a] | Average $\overline{a_i}$ | RMS $\sigma_{a_i}$ (%) | min($a_i$) / max($a_i$) | max($a_i$)-min($a_i$) (%) |
|---|---|---|---|---|---|---|
| B3 | 12mC | 6 | 0.989 | 2.4 | 0.937 / 1.009 | 7 |
| B3 | 12mE | 6 | 1.000 | 12.4 | 0.789 / 1.123 | 34 |
| B4 | 7m | 7 | 1.000 | 1.3 | 0.980 / 1.021 | 4 |
| B4 | 12m | 7 | 1.000 | 1.7 | 0.968 / 1.026 | 6 |
| B5 | 7m | 8 | 1.000 | 2.3 | 0.955 / 1.033 | 8 |
| B5[b] | 12m | 8 | 0.911 | 2.3 | 0.856 / 1.147 | 29 |
| B6 | 7m | 10 | 0.974 | 4.7 | 0.867 / 1.027 | 16 |
| B6 | 12m | 10 | 1.003 | 1.2 | 0.990 / 1.034 | 4 |
| B7 | 7m | 16 | 1.006 | 8.1 | 0.833 / 1.257 | 42 |
| B7 | 12m | 16 | 1.001 | 2.5 | 0.956 / 1.044 | 9 |

**Notes.** [(a)]Total number of scheduling block measurements included in the subsequent statistics shown. [(b)]Excludes 12m Array SB B5f as the scaling factor for this SB appears to include amplitude calibration errors inherent in the delivered calibrated data products.

and primary flux standard model calibration uncertainties (listed as in Sect. C.1):

- Band 3: 5% / 13% / 13%
- Band 4: 5% / 5% / 5%
- Band 5: 5% / 5% / 5%
- Band 6: 11% / 10% / 11%
- Band 7: 13% / 10% / 13%

Therefore, for the sake of simplicity, we recommend the usage of a conservative 15% uncertainty for the absolute flux calibration within the ALCHEMI image cubes, at any frequency and configuration.

### *C.3. A Search for the ALCHEMI Flux Normalization Anomalies*

We find that 11 of the 47 tunings (~23%) which comprise the ALCHEMI data set have amplitude scale factors which are larger than the ALMA amplitude calibration specification of 5%, with the two most discrepant tunings being 26% (Band 7) and 21% (Band 3). Table C.2 lists the measurement information for the 11 discrepant tunings.

In an attempt to determine the source(s) of the thirteen science goals with poor amplitude calibration, we have investigated how ALMA calibrates amplitude within the limits of the information provided to investigators. ALMA flux calibration is made within a given observation (or "execution block") by measurement of a standard quasar selected from a list of monitored quasars, referred to as the "grid sources". ALMA strives to measure these standard quasars at least once every 14 days at bands 3 and 7, and calibrates their fluxes to an absolute scale through reference measurements of primary flux calibrators (i.e., Uranus). The measured absolute fluxes for the grid source calibrators are available from the ALMA calibrator archive. We have extracted the flux scaling information from the calibration pipeline weblog file "flux.csv" associated with each observing execution block (EB). This flux scaling information includes the "spectral index age" and time since the standardized flux for each calibrator was derived.

#### C.3.1. Possible Source of Error: Large Spectral Index Age (spixAge)

As the spectral index age (spixAge) is one of the factors used by getALMAFlux to extrapolate measured flux calibrator fluxes to target frequencies, there was a concern that perhaps large spixAge factors were causing the large flux calibration errors. Using the spectral index age information extracted from the pipeline calibration process we show the correlation between spectral index age and amplitude scale factor in Figure C.1. There is no correlation between spixAge and the amount of the flux calibration error.

#### C.3.2. Possible Source of Error: Calibrator Catalog Band 3 Age

By inspecting the age of the absolutely calibrated Band 3 flux used by getALMAFlux (extracted from the flux.csv files associated with the pipeline calibration process), we find that there is no apparent correlation between the "Age"/"Band3Age" and large amplitude scaling factors. The "Age" or "Band3Age" is in almost all cases between 0 and 3 days for our most discrepant scale factor EBs. In one case it was 6 days, and another was 5 days, but neither of these were from our "worst cases". Band 3 age does not appear to be a likely source for the discrepant amplitude scale factors.

#### C.3.3. Possible Source of Error: Flux Monitoring Time Gaps

Many, though not all, of the science goals (SGs) with discrepant amplitude scale factors occur just after a gap in the respective flux calibrator measurements. Specifically, for 8 of the 13 discrepant Band 3 SGs, there was a significant flux calibrator measurement time gap just before these SGs were observed, and this correlation between flux calibrator measurement time gap and discrepant scale factor does not exist for Band 6 (green) or Band 7 (black) SGs with discrepant amplitude scale factors. Although this may be an explanation for the excessive Band 3 flux calibration uncertainties, a time gap in the flux monitoring for our flux calibrators does not appear to be consistent for all SGs with discrepant flux calibration.

#### C.3.4. Possible Source of Error: Large Time Span Between System Temperature Measurements

By perusing the weblogs associated with the ALCHEMI measurements we know that the scaling from raw amplitude to a temperature scale (otherwise known as the "system temperature" measurement), was routinely made only every ~11 minutes

**Table C.2.** ALCHEMI tunings with discrepant amplitude calibration

| SG[a] | Array | Flux Calibrators | SpixAge[b] | $100 \times \left\lvert \frac{\sigma_{gain}}{S_{gain}} \right\rvert^{c}$ | $a_i{}^{d}$ |
|---|---|---|---|---|---|
| B7d | 7m | J2258−2758,J0006−0623,J0522−3627 | (3,-4,20),(-4,20),20 | 9.98 | 1.257 |
| B3b | 12mE | J2258−2758 | 142,144 | 0.86 | 0.789 |
| B7h | 7m | J2258−2758,J2253+1608,J0522−3627 | (3,4),25,4 | 9.87 | 0.833 |
| B6f | 7m | J2253+1608 | -1,0,6 | 1.98 | 0.867 |
| B3d | 12mE | J0006−0623 | 7 | 1.57 | 1.128 |
| B3a | 12mE | J0006−0623 | -5,4 | 0.05,0.68 | 1.108 |
| B3c | 12mE | J0006−0623 | -3,-6,0,1 | 0.48 | 1.107 |
| B7o | 7m | J2253+1608,J0522−3627 | (7,0,2,3),2 | 2.06 | 0.922 |
| B3f | 12mE | J2258−2758,J2357−5311,J0006−0623 | -27,-22,4 | 1.84 | 0.922 |
| B6h | 7m | J2258−2758 | 5,-3,0,-2 | 3.71,1.03,1.20,4.30 | 0.924 |
| B3a | 12mC | J0006−0623 | 23,27 | 0.24 | 0.937 |

**Notes.** [a]Refers to Science Goals within ALMA project nomenclature. [b]Number of days since the most recent ALMA-derived spectral index for a given calibrator. Multiple executions which used a given calibrator are grouped within parentheses. Negative values indicate spectral indices derived before a given calibrator measurement. Calibrator spectral indices are derived using measured Band 3 and Band 6 or Band 7 fluxes. [c]Normalized gain calibrator flux uncertainty averaged over all gain calibrator measurements for observation dates within five days. Multiple entries indicate multiple observation time ranges. Target for all gain calibration measurements was J0038−2459. [d]Amplitude scale factors are applied to the data as indicated by Equation 3.

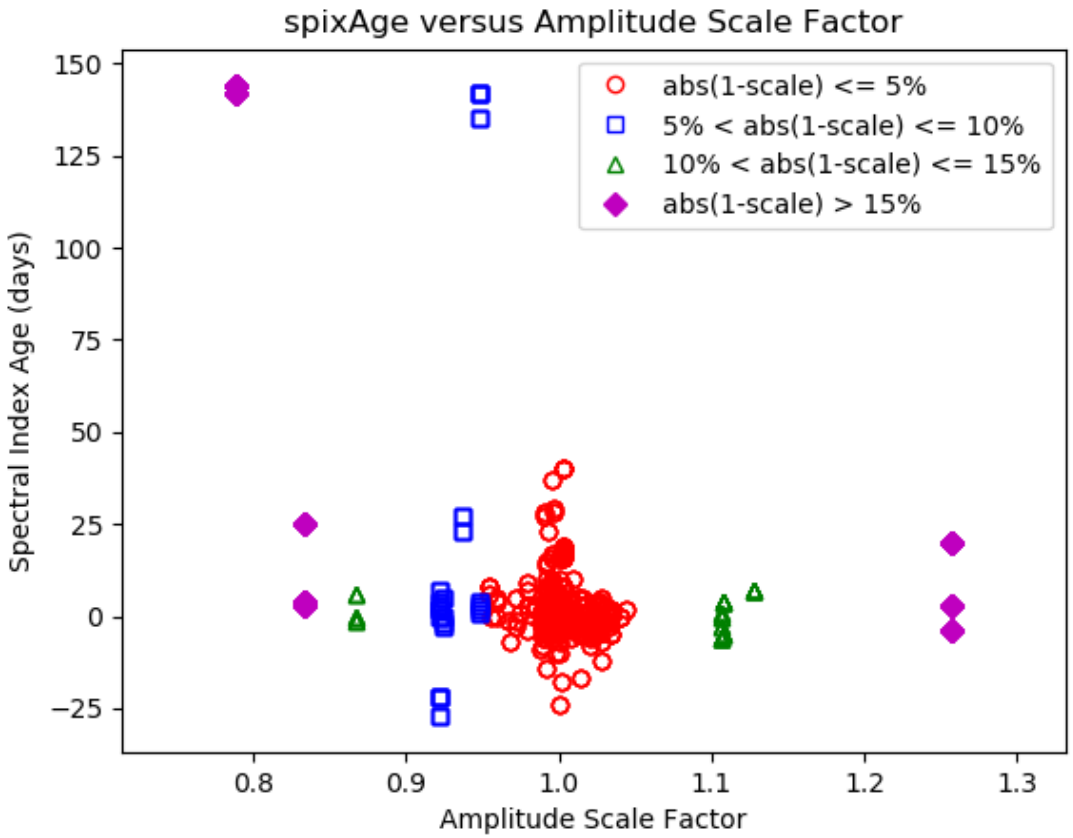


**Fig. C.1.** Correlation between spectral index age and amplitude scale factor for all ALCHEMI measurements. Coloring is used to designate ranges of amplitude scaling.

at Band 3 and every ∼8 minutes at Band 7. As these system temperature measurements are required to track the changes in sky emission as a function of time, it could be that these basic amplitude scaling factors have not been sampled well enough in time, especially at the higher frequency bands. However this is an observatory trade-off between enhanced calibration accuracy and observing efficiency.

#### C.3.5. Possible Source of Error: Noisy Gain Calibrator Measurement

For the SG with the most discrepant flux calibration, B7d 7m (ngc253_d_07_7M) there may be an issue with gain calibrator phase stability. Three out of five execution blocks (EBs) for the scheduling block (SB) were taken on the same day

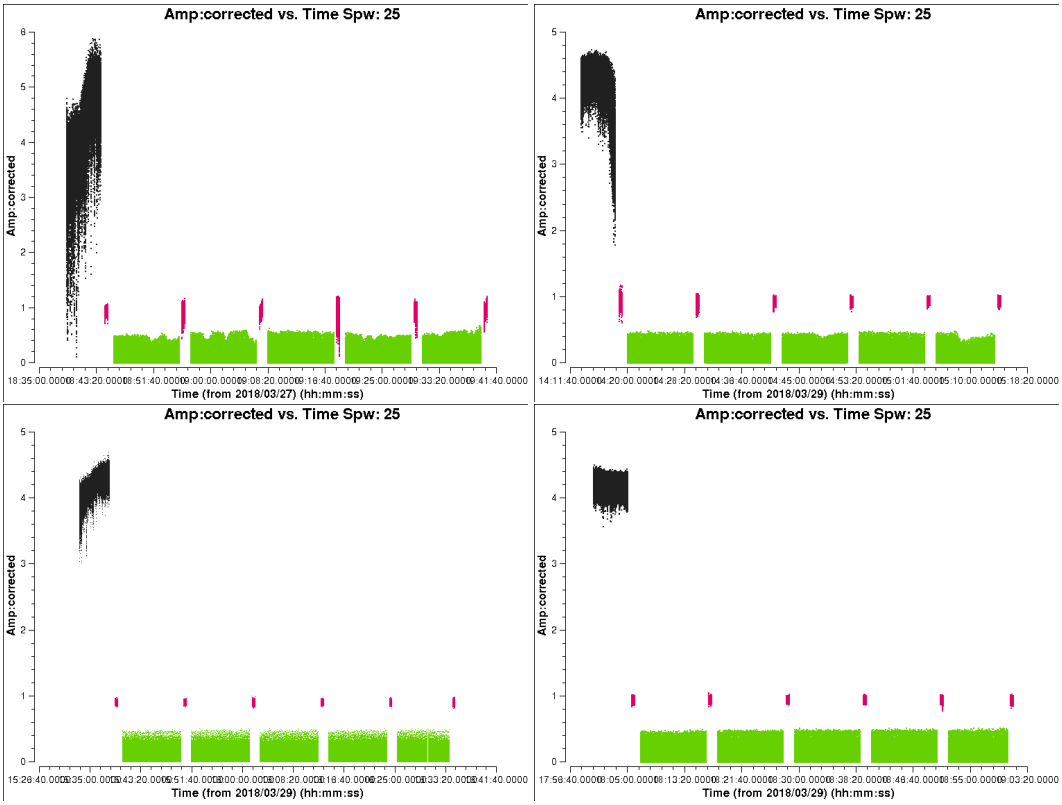


**Fig. C.2.** B3b 7m amplitude/bandpass calibrator flux versus time weblog plots for the four EBs in this SB.

(2018-01-21). J0038−2459 was observed as the gain calibrator for all the three EBs. Although the gain calibrator flux is expected to be stable over the three EBs, because the flux is very likely to be stable over the short time scale between these three EBs (about six hours), the derived flux densities in the pipeline calibration changed about 28% (peak-to-peak). The following is a summary of the pipeline-derived flux densities of the phase calibrator (reference: the weblog, stage 15).

```
# EB                      start date/time (UT)
 flux density (spw 16)
uid___A002_Xc96f17_X8658  2018-01-21 19:06:14
 1024.0+-9.979 mJy
uid___A002_Xc96f17_X8ec1  2018-01-21 22:17:40
 855.121+-12.804 mJy
uid___A002_Xc96f17_X92b9  2018-01-21 23:53:08
 797.500+-5.496 mJy
```

It is possible that poor atmospheric phase stability is the cause of the large flux calibration uncertainty, as all the EBs were taken in the late afternoon to early evening, which is the part of the day when the atmospheric phase stability tends to be very the poorest. In fact, in the calibrated visibility amplitude vs time plot of the EB (weblog stage 17) one can see frequent amplitude drops in the Bandpass/Flux calibrator scan.

Another example of a correlation between poor phase stability and poor flux calibration is B3b 12mE (ngc253_b_03_TM1). As was the case for B7d 7m, the EBs for this SB were also affected by large phase fluctuations, and that they were also executed in daytime (late afternoon). Figure C.2 shows the pipeline plots of amplitude vs time for all the EBs for B3b 7m. Significant amplitude drops in the bandpass/amplitude calibrator (J2258−2758) can be seen especially in EB uid___A002_Xcb1740_X94c9, and they could affect the flux scaling of the gain calibrator.

The following is a summary of the pipeline-derived flux density of gain calibrator J0038−2459 (reference: the weblog, stage 15).

```
spw=25
uid___A002_Xcb1740_X94c9  2018-03-27 18:36:03
 955.851+-14.748 mJy
uid___A002_Xcb339b_X600b  2018-03-29 14:10:14
 938.721+-7.809 mJy
uid___A002_Xcb339b_X633f  2018-03-29 15:30:21
 903.452+-9.069 mJy
uid___A002_Xcb339b_X68ab  2018-03-29 17:57:08
 941.212+-1.904 mJy
```

The change of delivered flux density looks relatively large (5.8% in peak-to-peak) even though the EBs were taken within three days. This could be an explanation for the discrepant flux calibration (second worst of all SGs) for this SG.

In order to assess the effect of a large gain calibrator flux uncertainties on the derivation of our flux calibration uncertainty for all of the ALCHEMI SGs, we have extracted all derived gain calibrator fluxes and uncertainties from the ALCHEMI weblogs. We have derived a normalized gain calibration error for each SG by doing the following: Firstly, we calculate the weighted uncertainty ($\sigma_{gain}$) for all gain calibrator measurements; Secondly, we average normalized gain calibrator uncertainties ($\frac{\sigma_{gain}}{S_{gain}}$) over all spectral windows and measurements taken within 5 days of each other. This time window is expected to be shorter than any changes in the absolute flux of the gain calibrator; Finally, by using a normalized gain calibrator uncertainty, we are attempting to smooth-out any changes in gain calibrator flux measurement uncertainty due to differences in gain calibrator integration time.

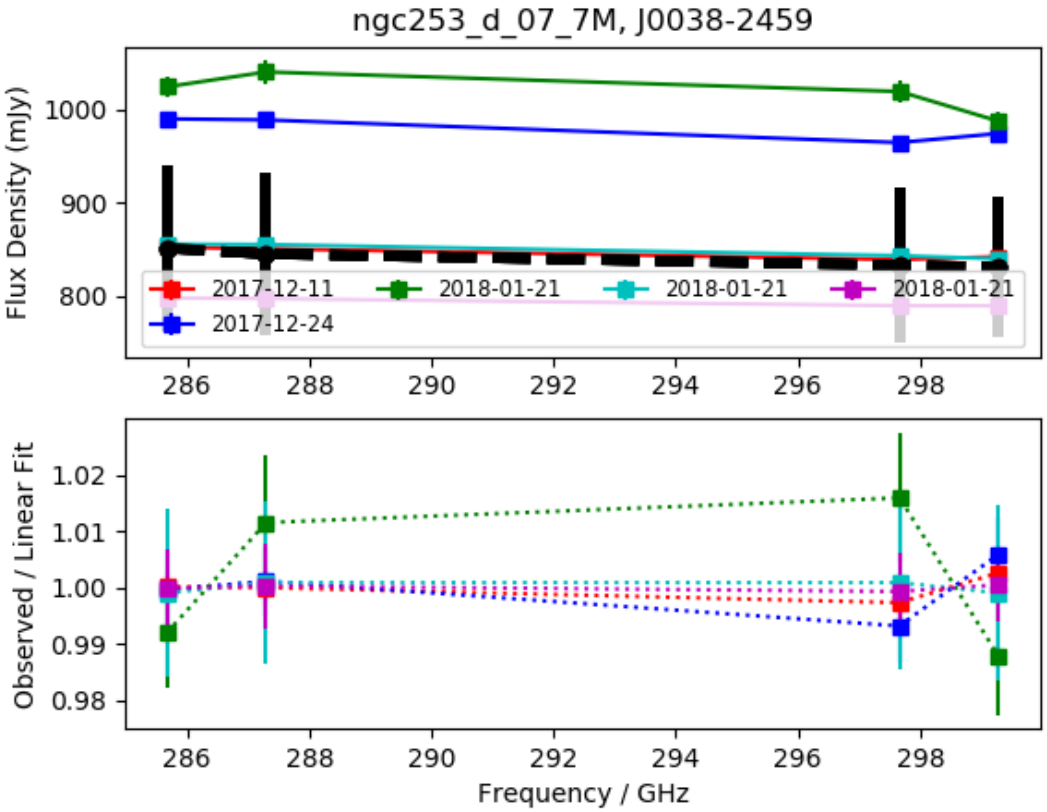


**Fig. C.3.** Sample gain calibration results for all EBs associated with B7d 7m. The bottom panel shows the residual from a linear fit for each measurement date to the measured flux densities displayed in the top panel.

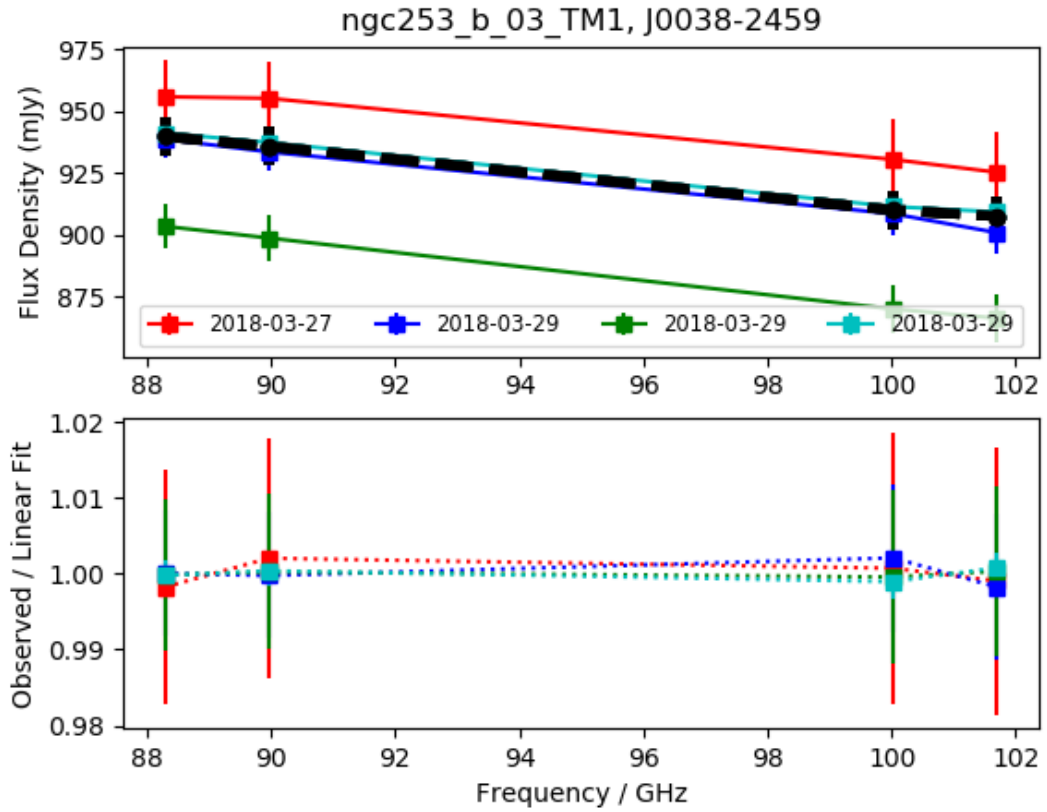


**Fig. C.4.** Sample gain calibration results for all EBs associated with B3b TM1. Same diagram style as used in Figure C.3.

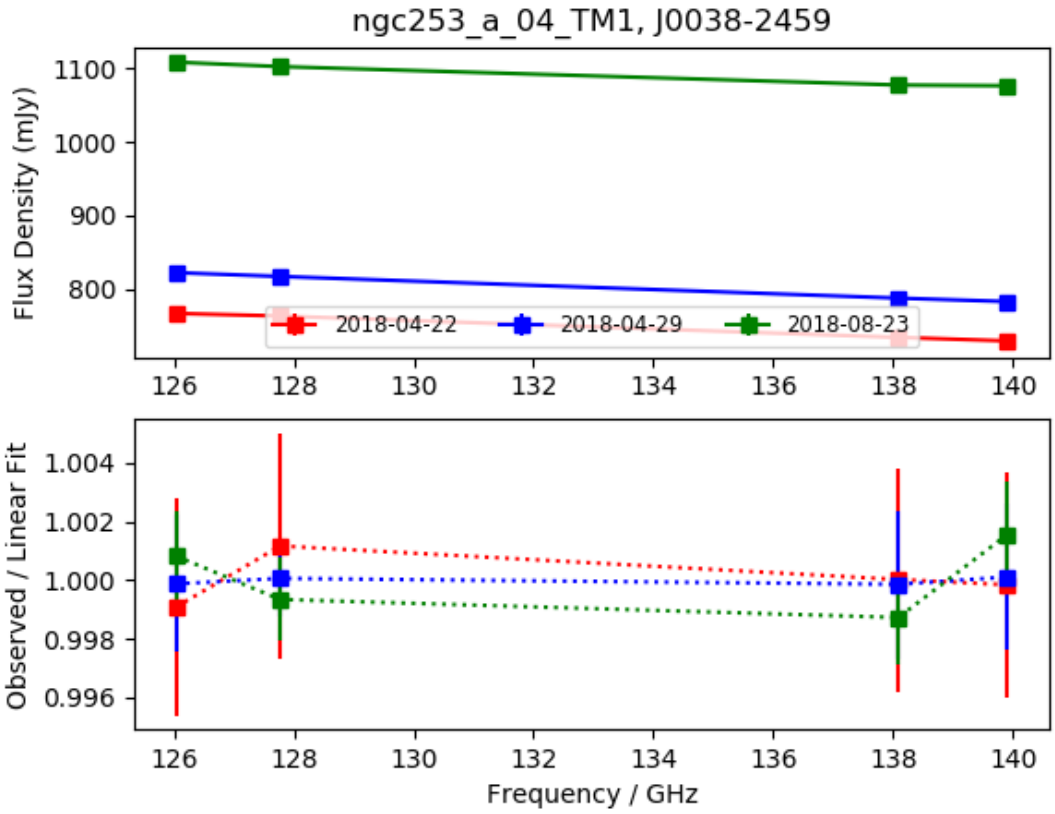


**Fig. C.5.** Sample gain calibration results for all EBs associated with B4a TM1. Same diagram style as used in Figure C.3.

Figures C.3, C.4, and C.5 show examples of gain calibrator measurements, with weighted uncertainties, and their associated weighted average as a function of frequency. Figure C.6 shows the correlation between normalized gain calibrator standard deviation (as a percentage) versus the associated amplitude calibration scale factor (calculated as a difference from a perfect amplitude scale factor of 1.0). Even though in a few cases large normalized gain calibration errors are associated with large amplitude scale factors, there is no systematic correlation between these measures.

### *C.4. Conclusion to Search for ALCHEMI Flux Normalization Anomalies*

In Sections C.3.1 through C.3.5 we have investigated the possible sources of the discrepant flux calibration uncertainties derived for 13 of the ALCHEMI SBs. We find that with the exception of possible errors in $T_{sys}$ measurement, which we are unable to properly analyze, none of the above potential sources of error appear to explain all of our discrepant amplitude calibration.

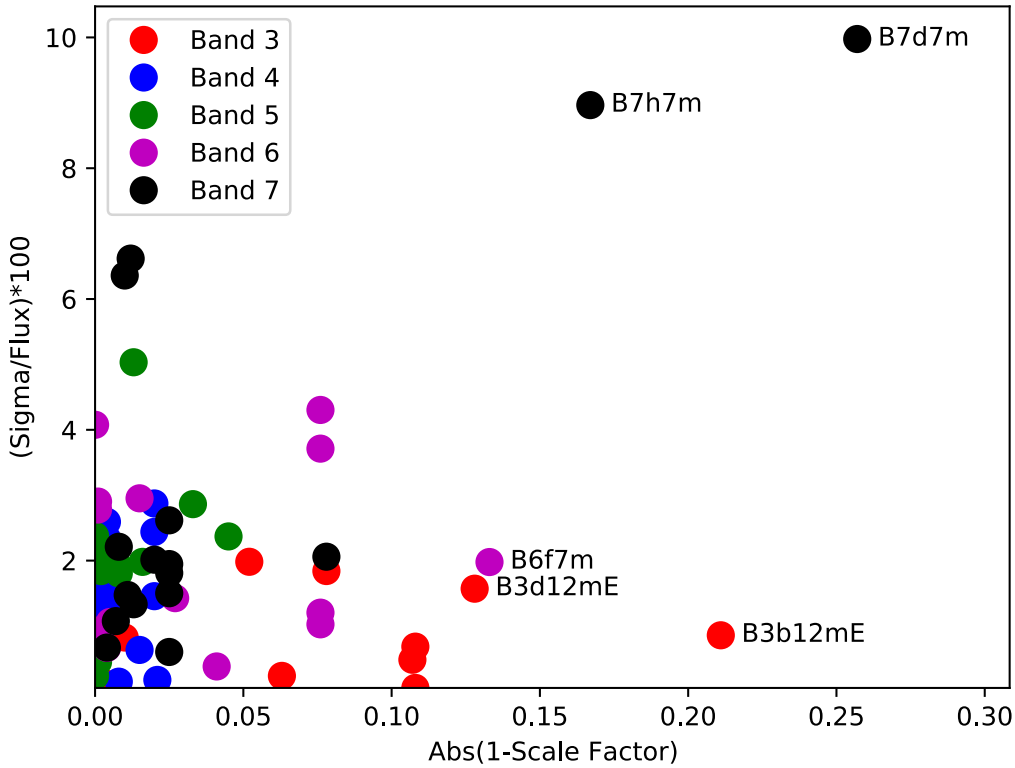


**Fig. C.6.** Correlation between normalized gain calibrator standard deviation (as a percentage) versus the associated amplitude calibration scale factor (calculated as a difference from a perfect amplitude scale factor of 1.0). Tunings with larger than 12% scale factors are annotated. See above description for calculation details.

## Appendix D: Fitting details of individual species

Sect. 4.3.2 provided details on the procedure used to fit the modeled synthetic spectra to the low resolution ACA observations. In summary, the procedure consists on a human-supervised automatic fit, where the only intervention aims at ensuring convergence of the fit. Additional criteria used for the newly detected species (Sect. 4.4) are provided below in Sect. D.1. Thus, parameters were fixed or transitions were masked in the fit when convergence could not be achieved. The results are reported in Table. A.3. Here we note that in some cases, the large uncertainty in the fit to the temperature resulted in column density errors of the same order as the value fitted. Such is the case of $H^{13}CN$, despite being a clear detection with bright features, extra masking and fixing of the temperature was required to provide a reasonably narrow error on the column density (with only marginal change in the fitted column density value). However in most cases we decided to maintain such fits for the sake of consistency with the procedure applied to all species.

Although we know from previous studies that there is evidence for the presence of multiple components with different excitation temperatures (Aladro et al. 2011b), there are no really obvious deviations from the LTE fit. As an example the higher energy transitions of $HC_3N$ appear to be underestimated, which could support the presence of a higher temperature component. Similarly $H_2CO$ is not that well fitted under LTE, showing flat topped spectral features. For the sake of simplicity in the presentation of these data, we assumed a single LTE component for all species. A detailed analysis of the excitation of some of these species will be presented in future publications which will make use of the higher resolution ALCHEMI 12m Array data.

For the sake of completeness, a list of all transitions above a peak flux density of 15 mJy are presented in Table D.1. We note that these intensities correspond to those of the model fit to the observed spectra, and therefore parameters of velocity and width are those corresponding to the species as presented in Table A.3. As indicated in Sect. 4.3.2, no measurement or analysis of individual spectral features has been performed. For the reasons presented there, analysis has been performed per molecular species.

Below we provide some cases of transitions significantly deviating from LTE together with other special details on the fitting of individual species.

$H_3O^+$ : The fit to $H_3O^+$ emission has been performed only on the 307.2 GHz transition, which is one of the two transitions covered by our survey. Although the 307.2 GHz is blended with $CH_3OH$, this contribution is accounted for based on the $CH_3OH$ fit to the whole survey. The 364.8 GHz transition, on the other hand, is the most obvious case of non-LTE emission, and is observed to be more than an order of magnitude brighter than predicted by LTE (Fig. F.11) The line ratio between these two transitions has been calculated based on the individual integrated intensity fit to each transition and not on the LTE intensities in Table. D.1. To explain the relatively large observed flux density ratio of $S_{364.8}/S_{307.2} = 6.8 \pm 1.0$ between the two transitions, non-LTE models from Phillips et al. (1992) suggest volume densities $< 10^7 cm^{-3}$ and effective excitation by dust emission. Together with the vibrational emission reported in Sect. 5.2, $H_3O^+$ is also probing the importance of infrared pumping in NGC 253 GMCs. However, the 396 GHz transition of $H_3O^+$, not covered in our survey, is key to constrain the non-LTE physical conditions of the emitting gas. All other species below that show transitions not well fitted by the LTE approximations, are not as extreme as the case of $H_3O^+$ where, as mentioned

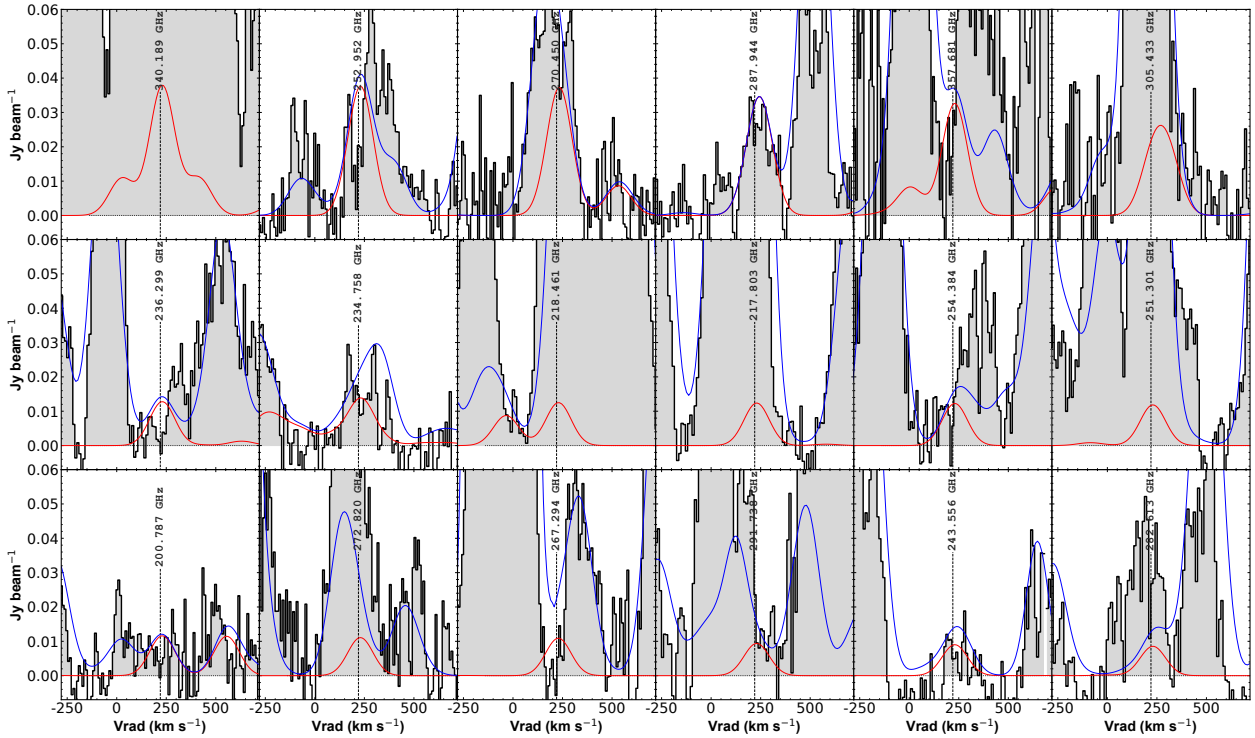


**Fig. D.1.** Modeled emission of $C_2H_5OH$ in red, overlaid over the observed spectrum (filled black histogram) and the global model including all molecular transitions in this study. Only the 18 brightest transitions or group of transitions according to the LTE model of $C_2H_5OH$ are displayed, ordered in descending order of brightness from left to right and top to bottom. The model generated with MADCUBA makes use of the spectroscopic parameters in JPL catalog entry 46004. The frequency of the brightest transition in each panel are displayed for reference.

above, the LTE approximation is underestimating the 364.8 GHz by more than an order of magnitude.

*$H_2S$* : The transition of $H_2S$ at 216.71 GHz is approximately two times brighter than predicted by the LTE fit.

*$H_2CO$* : The transitions at 140.83 and 150.48 GHz are twice as bright as predicted by the LTE fit. A number of other transitions also deviate from the fit, but to a lesser extent. We note that we did not fit the ortho- and para-$H_2CO$ separately, but we assumed the ortho-to-para ratio of 3.

*$HC_3N$* : All transitions above 270 GHz are brighter than the LTE fit estimate. This could be the signature of a warmer component and partially to the effect of varying opacity across the transitions.

*$HNCO$* : The brighter transitions of HNCO show an obvious double peak profile which is likely due to the distribution of this species at high resolution (Meier et al. 2015). This double peak profile, similarly observed in $CH_3OH$, is more apparent than in other species where the velocity components are more blended and the profile is a single peak. On the other hand, many of the fainter transitions of HNCO are overestimated by the LTE fit.

*$CH_3^{13}CCH$* : Despite being almost uniformly blended with other species, the fit of $CH_3^{13}CCH$ is consistent within the errors to that of the other two isotopologues, being ∼0.1 dex above $CH_3C^{13}CH$ and ∼0.4 dex above $^{13}CH_3CCH$. Although the uncertainties in the column density determination of the latter two isotopologues are of the same order as the value fitted, an independent fit to the three isotopologues are in good agreement, which supports the detection and fit to those species. Moreover, the ratio to the main isotopologue (Table 4) is consistent with what is observed with other species as discussed in Sect. 5.4.1).

*$CH_3OH$* : Two of the transitions of methanol, the $1_{1,0}-2_{0,2}$ at 205.79 GHz and $7_{1,7}-6_{1,6}$ at 335.58 GHz, show observed fluxes which are less than half of the LTE fit flux, while the $6_{1,5}-5_{1,4}$ at 292.7 GHz transition is about half of the LTE fit flux. Similar to what is observed in HNCO, the brighter transitions show a very clear double peak profile.

*$^{13}CH_3OH$* : There is only one transition of $^{13}CH_3OH$ which is bright enough and is not blended with other species. Therefore this is the only species in which the fit value should be considered with caution and probably an upper limit. This LTE fit has been discussed in Sect. 5.4.1.

*$CH_3CN$* : The $J = 7-6$ and $8-7$ groups of transitions at 128.7 and 147.1 GHz, respectively, show significantly brighter emission than that from the LTE fit, being up to a factor of two brighter on the former.

*$CH_2NH$* : While the $3_{1,1}-1_{0,1}$ transition at 166.85 GHz is not detected, though predicted by the LTE fit, the $2_{0,2}-1_{0,1}$ transition at 127.85 GHz is brighter than predicted.

### *D.1. Fitting details of newly detected species*

On top of the fit criteria explained in Sect. 4.3.2 on detection of the brightest spectral features and requiring convergence of the fit, we enforced extra criteria to claim newly detected species. This is, at least one of the brightest (according to the LTE prediction) spectral features needs to be un-blended or marginally contaminated by emission from other species based on the LTE modeling to other transitions from the contaminant species. More importantly, all other blended transitions should be consistent with the residual spectra after subtraction of all other modeled species. In other words, any bright emission line predicted

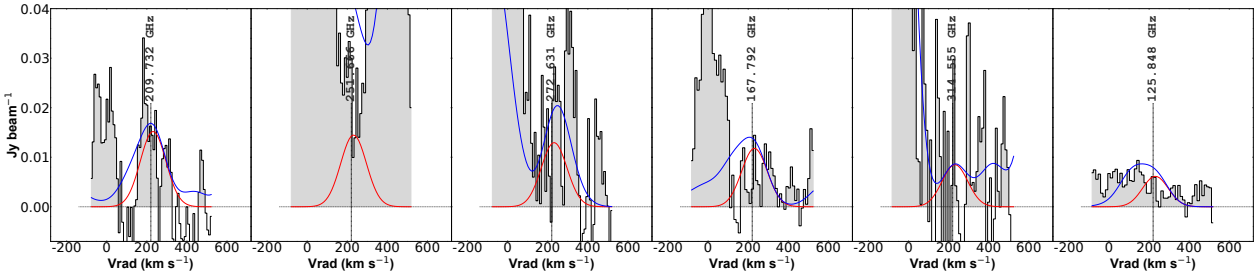


**Fig. D.2.** Same as Fig. D.1 showing the model of HOCN, using the spectroscopic parameters in CDMS catalog entry 43510.

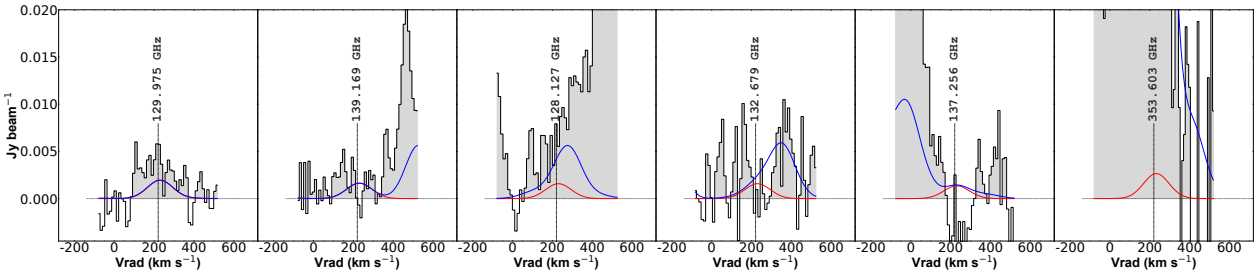


**Fig. D.3.** Same as Fig. D.1 showing the model of $HC_3HO$, using the spectroscopic parameters in JPL catalog entry 54007.

**Table D.1.** Intensities from the 744 transitions with > 15 mJy from the LTE model fit to the data

| Formula | $\nu$ (GHz) | $S$ (mJy) | Formula | $\nu$ (GHz) | $S$ (mJy) | Formula | $\nu$ (GHz) | $S$ (mJy) | Formula | $\nu$ (GHz) | $S$ (mJy) |
|---|---|---|---|---|---|---|---|---|---|---|---|
| H$\beta$ | 126.794 | 24 | HNCO | 198.529 | 22 | H$\alpha$ | 256.302 | 86 | He$\alpha$ | 316.544 | 32 |
| $HC_3N$ | 127.368 | 213 | HNCO | 198.529 | 25 | $CH_3C_2H$ | 256.317 | 71 | $CH_2NH$ | 317.405 | 64 |
| $CH_3CN$ | 128.779 | 29 | HNCO | 198.529 | 28 | $CH_3C_2H$ | 256.332 | 120 | $CH_2NH$ | 317.405 | 78 |
| SO | 129.139 | 27 | $CH_2NH$ | 199.823 | 34 | $CH_3C_2H$ | 256.337 | 142 | c-$C_3H_2$ | 318.294 | 34 |
| SiO | 130.269 | 71 | $HC_3N$ | 200.135 | 189 | He$\alpha$ | 256.406 | 27 | $CH_3OH$ | 318.319 | 74 |
| HNCO | 131.886 | 59 | $H_2C_2N$ | 201.144 | 31 | $^{29}$SiO | 257.255 | 20 | c-$C_3H_2$ | 318.482 | 93 |
| HNCO | 131.886 | 49 | $CH_3CN$ | 202.34 | 35 | $CH_3CN$ | 257.508 | 39 | c-$C_3H_2$ | 318.79 | 30 |
| HNCO | 131.886 | 41 | $CH_3CN$ | 202.356 | 77 | $CH_3CN$ | 257.527 | 83 | $HC_3N$,v7=1 | 319.576 | 36 |
| $CH_3OH$ | 132.891 | 15 | $H_2CS$ | 202.924 | 39 | $HC^{15}N$ | 258.157 | 63 | $NH_2CN$ | 321.93 | 19 |
| $C_3H^+$ | 134.933 | 22 | c-$C_3H_2$ | 204.789 | 19 | SO | 258.256 | 150 | $CH_3OH$ | 322.239 | 35 |
| H$\beta$ | 135.249 | 26 | $CH_3C_2H$ | 205.045 | 53 | $H^{13}CN$ | 259.012 | 105 | $C_2H_5OH$ | 322.691 | 21 |
| H$\alpha$ | 135.286 | 50 | $CH_3C_2H$ | 205.065 | 64 | $H^{13}CN$ | 259.012 | 152 | $C_2H_5OH$ | 322.691 | 21 |
| He$\alpha$ | 135.341 | 15 | $CH_3C_2H$ | 205.077 | 108 | $H^{13}CN$ | 259.012 | 71 | $CH_3NH_2$ | 323.462 | 16 |
| $HC_3N$ | 136.464 | 231 | $CH_3C_2H$ | 205.081 | 129 | H$\beta$ | 260.033 | 46 | $^{13}$CS | 323.685 | 19 |
| $CH_3C_2H$ | 136.705 | 21 | H$\beta$ | 205.76 | 38 | $H^{13}CO^+$ | 260.255 | 339 | $CH_3C_2H$ | 324.607 | 42 |
| $CH_3C_2H$ | 136.718 | 27 | $CH_3OH$ | 205.791 | 272 | SiO | 260.518 | 193 | $CH_3C_2H$ | 324.638 | 49 |
| $CH_3C_2H$ | 136.725 | 47 | $H_2CS$ | 205.987 | 21 | $CH_3NH_2$ | 261.219 | 34 | $CH_3C_2H$ | 324.657 | 81 |
| $CH_3C_2H$ | 136.728 | 56 | SO | 206.176 | 98 | $HN^{13}C$ | 261.263 | 173 | $CH_3C_2H$ | 324.663 | 97 |
| SO | 138.179 | 73 | OCS | 206.745 | 35 | $NH_2CN$ | 261.594 | 20 | $CH_3NH_2$ | 325.531 | 50 |
| $^{13}$CS | 138.739 | 34 | $CH_2NH$ | 207.38 | 15 | $CH_3OH$ | 261.806 | 128 | $^{13}$CN | 325.943 | 30 |
| $H_2CO$ | 140.84 | 135 | NS | 207.436 | 30 | SO | 261.844 | 264 | $^{13}$CN | 325.956 | 21 |
| $H_2C_2N$ | 140.84 | 36 | NS | 207.835 | 39 | $C_2H$ | 262.004 | 1153 | $^{13}$CN | 325.958 | 31 |
| $CH_3OH$ | 143.866 | 33 | NS | 207.838 | 24 | $C_2H$ | 262.006 | 876 | $^{13}$CN | 326.119 | 42 |
| H$\beta$ | 144.474 | 28 | $C_2S$ | 208.216 | 15 | $C_2H$ | 262.065 | 837 | $^{13}$CN | 326.125 | 19 |
| $C^{34}S$ | 144.617 | 92 | $H_2CS$ | 209.2 | 41 | $C_2H$ | 262.067 | 555 | $^{13}$CN | 326.142 | 57 |
| c-$C_3H_2$ | 145.09 | 48 | $HC_3N$ | 209.23 | 167 | $C_2H$ | 262.079 | 76 | $^{13}$CN | 326.143 | 33 |
| $CH_3OH$ | 145.094 | 40 | HOCN | 209.732 | 15 | $C_2H$ | 262.208 | 70 | $CH_3OH$ | 326.631 | 15 |
| $CH_3OH$ | 145.097 | 49 | H$\alpha$ | 210.502 | 74 | HNCO | 262.77 | 26 | $CH_3OH$ | 326.961 | 15 |
| $CH_3OH$ | 145.103 | 69 | He$\alpha$ | 210.588 | 23 | HNCO | 262.77 | 24 | OCS | 328.298 | 25 |
| $CH_3OH$ | 145.126 | 15 | $H_2CO$ | 211.211 | 410 | HNCO | 262.77 | 22 | $HC_3N$,v7=1 | 328.701 | 38 |
| $CH_3OH$ | 145.132 | 26 | $CH_3OH$ | 213.427 | 56 | HNCO | 263.749 | 117 | $CH_3NH_2$ | 329.199 | 51 |
| $HC_3N$ | 145.561 | 243 | $HOCO^+$ | 213.813 | 18 | HNCO | 263.749 | 108 | $C^{18}O$ | 329.331 | 4461 |
| $H_2CO$ | 145.603 | 147 | $CH_3NH_2$ | 215.108 | 26 | HNCO | 263.749 | 99 | HNCO | 329.665 | 63 |
| $C^{33}S$ | 145.756 | 19 | SO | 215.221 | 115 | $HC_3N$ | 263.792 | 52 | HNCO | 329.665 | 58 |
| OCS | 145.947 | 17 | c-$C_3H_2$ | 216.279 | 155 | $CH_3NH_2$ | 264.172 | 32 | HNCO | 329.665 | 55 |
| $CH_3OH$ | 146.368 | 34 | $H_2S$ | 216.71 | 98 | HNCO | 264.694 | 26 | $^{13}$CO | 330.588 | 13300 |
| CS | 146.969 | 880 | $CH_3OH$ | 216.946 | 19 | HNCO | 264.694 | 22 | $CH_3CN$ | 331.046 | 23 |
| H$\alpha$ | 147.047 | 54 | SiO | 217.105 | 191 | HNCO | 264.694 | 24 | $CH_3CN$ | 331.072 | 50 |
| He$\alpha$ | 147.107 | 17 | $^{13}$CN | 217.303 | 44 | $HC_3N$,v7=1 | 264.817 | 22 | $SO_2$ | 332.505 | 19 |

**Table D.1.** continued.

| Formula | $\nu$ (GHz) | $S$ (mJy) | Formula | $\nu$ (GHz) | $S$ (mJy) | Formula | $\nu$ (GHz) | $S$ (mJy) | Formula | $\nu$ (GHz) | $S$ (mJy) |
|---|---|---|---|---|---|---|---|---|---|---|---|
| $CH_3CN$ | 147.163 | 19 | $^{13}CN$ | 217.436 | 19 | $CH_3OH$ | 265.29 | 27 | $CH_2NH$ | 332.573 | 39 |
| $CH_3CN$ | 147.175 | 42 | $^{13}CN$ | 217.467 | 41 | HCN,v2 | 265.853 | 47 | $CH_2NH$ | 332.573 | 31 |
| $HOCO^+$ | 149.676 | 27 | c-$C_3H_2$ | 217.822 | 69 | HCN | 265.886 | 6477 | $CH_3NH_2$ | 333.839 | 17 |
| NO | 150.176 | 23 | c-$C_3H_2$ | 217.822 | 207 | $CH_2NH$ | 266.27 | 39 | $CH_3NH_2$ | 334.712 | 17 |
| $H_2CO$ | 150.498 | 158 | c-$C_3H_2$ | 217.94 | 157 | $CH_2NH$ | 266.27 | 30 | $CH_3OH$ | 335.134 | 31 |
| NO | 150.547 | 23 | c-$C_3H_2$ | 218.16 | 52 | $H^{15}NC$ | 266.588 | 16 | H$\beta$ | 335.207 | 55 |
| c-$C_3H_2$ | 150.852 | 126 | $H_2CO$ | 218.222 | 369 | $CH_3OH$ | 266.838 | 117 | $CH_3OH$ | 335.582 | 136 |
| HNCO | 153.292 | 18 | $HC_3N$ | 218.325 | 144 | HCN,v2 | 267.199 | 48 | $C^{17}O$ | 337.061 | 617 |
| HNCO | 153.292 | 16 | $CH_3NH_2$ | 218.409 | 23 | OCS | 267.53 | 37 | $CH_3NH_2$ | 337.119 | 18 |
| $CH_3C_2H$ | 153.791 | 30 | $CH_3OH$ | 218.44 | 93 | $HCO^+$ | 267.558 | 7021 | $C^{34}S$ | 337.397 | 175 |
| $CH_3C_2H$ | 153.805 | 37 | $NH_2CN$ | 218.462 | 16 | $HOC^+$ | 268.451 | 240 | $HC_3N$,v7=1 | 337.825 | 40 |
| $CH_3C_2H$ | 153.814 | 63 | OCS | 218.903 | 37 | $C_2H_5OH$ | 270.444 | 18 | $H_2CS$ | 338.081 | 49 |
| $CH_3C_2H$ | 153.817 | 76 | HNCO | 218.981 | 29 | $C_2H_5OH$ | 270.451 | 18 | $CH_3OH$ | 338.124 | 147 |
| HNCO | 153.865 | 62 | HNCO | 218.981 | 26 | $H_2CS$ | 270.521 | 56 | c-$C_3H_2$ | 338.204 | 100 |
| HNCO | 153.865 | 72 | HNCO | 218.981 | 24 | HNC | 271.981 | 3903 | $CH_3OH$ | 338.345 | 197 |
| HNCO | 153.865 | 84 | $C^{18}O$ | 219.56 | 2380 | $HC_3N$ | 272.885 | 40 | $CH_3OH$ | 338.409 | 254 |
| HNCO | 154.415 | 16 | HNCO | 219.798 | 130 | $CH_3C_2H$ | 273.373 | 58 | $CH_3OH$ | 338.513 | 49 |
| HNCO | 154.415 | 19 | HNCO | 219.798 | 106 | $CH_3C_2H$ | 273.399 | 68 | $CH_3OH$ | 338.541 | 26 |
| H$\beta$ | 154.557 | 29 | HNCO | 219.798 | 117 | $CH_3C_2H$ | 273.415 | 114 | $CH_3OH$ | 338.543 | 26 |
| $HC_3N$ | 154.657 | 249 | SO | 219.949 | 217 | $CH_3C_2H$ | 273.42 | 136 | $CH_3OH$ | 338.56 | 15 |
| c-$C_3H_2$ | 155.518 | 26 | $^{13}CO$ | 220.399 | 7383 | $HC_3N$,v7=1 | 273.945 | 24 | $CH_3OH$ | 338.583 | 28 |
| $CH_3OH$ | 156.602 | 53 | HNCO | 220.585 | 29 | $H_2CS$ | 274.521 | 29 | $CH_3OH$ | 338.615 | 106 |
| $CH_3OH$ | 156.829 | 15 | HNCO | 220.585 | 24 | $H_2{}^{13}CO$ | 274.762 | 35 | $CH_3OH$ | 338.64 | 49 |
| $CH_3OH$ | 157.049 | 28 | HNCO | 220.585 | 26 | $CH_3CN$ | 275.894 | 36 | $CH_3OH$ | 338.722 | 92 |
| $CH_3OH$ | 157.179 | 44 | $CH_3CN$ | 220.73 | 38 | $CH_3CN$ | 275.916 | 78 | $CH_3OH$ | 338.723 | 80 |
| $CH_3OH$ | 157.246 | 60 | $CH_3CN$ | 220.747 | 83 | $^{13}CS$ | 277.455 | 37 | SO | 339.341 | 18 |
| $CH_3OH$ | 157.271 | 50 | $H_2C_2N$ | 221.254 | 20 | $CH_3OH$ | 278.305 | 22 | CN | 339.447 | 52 |
| $CH_3OH$ | 157.272 | 70 | $NH_2CN$ | 221.361 | 17 | $CH_3OH$ | 278.342 | 31 | CN | 339.476 | 74 |
| $CH_3OH$ | 157.276 | 68 | H$\beta$ | 222.012 | 40 | $H_2CS$ | 278.886 | 58 | CN | 339.517 | 117 |
| OCS | 158.107 | 21 | $CH_3C_2H$ | 222.129 | 58 | $N_2H^+$ | 279.512 | 1339 | $CH_3NH_2$ | 339.724 | 56 |
| SO | 158.972 | 46 | $CH_3C_2H$ | 222.15 | 69 | OCS | 279.685 | 36 | $^{34}SO$ | 339.858 | 16 |
| H$\alpha$ | 160.212 | 58 | $CH_3C_2H$ | 222.163 | 117 | $H_2CO$ | 281.527 | 544 | CN | 340.008 | 214 |
| He$\alpha$ | 160.277 | 18 | $CH_3C_2H$ | 222.167 | 139 | $NH_2CN$ | 281.708 | 20 | CN | 340.02 | 214 |
| $H_2C_2N$ | 160.949 | 38 | $C^{17}O$ | 224.714 | 323 | $HC_3N$ | 281.977 | 30 | CN | 340.032 | 1639 |
| NS | 161.298 | 19 | $C_3H^+$ | 224.868 | 15 | H$\beta$ | 282.333 | 49 | CN | 340.035 | 651 |
| NS | 161.697 | 26 | $CH_2NH$ | 225.554 | 51 | c-$C_3H_2$ | 282.381 | 93 | CN | 340.035 | 1068 |
| $HC_3N$ | 163.753 | 247 | $CH_2NH$ | 225.556 | 17 | $HC_3N$,v7=1 | 283.072 | 26 | $C^{33}S$ | 340.053 | 33 |
| $CH_3OH$ | 165.05 | 38 | $H_2CO$ | 225.698 | 456 | $H_2{}^{13}CO$ | 283.442 | 26 | $CH_3OH$ | 340.141 | 32 |
| $CH_3OH$ | 165.061 | 53 | CN | 226.287 | 57 | H$\alpha$ | 284.251 | 94 | $C_2H_5OH$ | 340.189 | 18 |
| $CH_3OH$ | 165.099 | 55 | CN | 226.299 | 46 | $CH_2NH$ | 284.253 | 27 | $C_2H_5OH$ | 340.189 | 18 |
| $CH_3OH$ | 165.19 | 48 | CN | 226.303 | 46 | $CH_2NH$ | 284.254 | 152 | CN | 340.248 | 2129 |
| $CH_3OH$ | 165.369 | 36 | CN | 226.315 | 110 | $CH_2NH$ | 284.255 | 27 | CN | 340.248 | 1615 |
| $CH_3CN$ | 165.556 | 25 | CN | 226.333 | 51 | He$\alpha$ | 284.366 | 29 | CN | 340.249 | 1201 |
| $CH_3CN$ | 165.569 | 55 | CN | 226.342 | 53 | HNCO | 284.662 | 23 | CN | 340.262 | 155 |
| H$\beta$ | 165.601 | 31 | CN | 226.36 | 265 | HNCO | 284.662 | 21 | CN | 340.265 | 154 |
| $CH_3OH$ | 165.679 | 23 | CN | 226.617 | 60 | HNCO | 284.662 | 19 | $CH_2NH$ | 340.353 | 16 |
| $H_2S$ | 168.763 | 265 | CN | 226.632 | 461 | c-$C_3H_2$ | 284.805 | 50 | $CH_2NH$ | 340.354 | 191 |
| $H_2CS$ | 169.114 | 25 | CN | 226.66 | 1399 | c-$C_3H_2$ | 284.998 | 132 | $CH_2NH$ | 340.355 | 16 |
| $CH_3OH$ | 170.061 | 57 | CN | 226.664 | 458 | $CH_3OH$ | 285.111 | 32 | $CH_3NH_2$ | 340.598 | 56 |
| OCS | 170.267 | 25 | CN | 226.679 | 565 | HNCO | 285.722 | 101 | $HC^{18}O^+$ | 340.633 | 69 |
| $HC^{18}O^+$ | 170.323 | 30 | CN | 226.874 | 1416 | HNCO | 285.722 | 93 | SO | 340.714 | 157 |
| $HCS^+$ | 170.692 | 24 | CN | 226.875 | 2077 | HNCO | 285.722 | 86 | $CH_3OH$ | 341.416 | 137 |
| $CH_3C_2H$ | 170.876 | 39 | CN | 226.876 | 890 | HNCO | 286.747 | 23 | $CH_3C_2H$ | 341.683 | 35 |
| $CH_3C_2H$ | 170.893 | 47 | CN | 226.887 | 299 | HNCO | 286.747 | 19 | $CH_3C_2H$ | 341.715 | 41 |
| $CH_3C_2H$ | 170.902 | 80 | CN | 226.892 | 297 | HNCO | 286.747 | 21 | $CH_3C_2H$ | 341.735 | 68 |
| $CH_3C_2H$ | 170.906 | 96 | $HC_3N$ | 227.419 | 122 | $CH_3OH$ | 287.671 | 142 | $CH_3C_2H$ | 341.741 | 81 |
| $HOCO^+$ | 171.056 | 27 | $CH_3OH$ | 229.759 | 25 | $C_2H_5OH$ | 287.918 | 17 | $NH_2CN$ | 342.038 | 17 |
| $HC^{15}N$ | 172.108 | 32 | $CH_3OH$ | 230.027 | 29 | $C_2H_5OH$ | 287.945 | 17 | CS | 342.883 | 1138 |
| SO | 172.181 | 68 | CO | 230.538 | 56226 | $C^{34}S$ | 289.209 | 228 | $H_2CS$ | 342.944 | 26 |
| $H^{13}CN$ | 172.677 | 15 | OCS | 231.061 | 38 | $CH_3OH$ | 289.939 | 155 | $CH_3SH$ | 343.048 | 15 |
| $H^{13}CN$ | 172.677 | 20 | $^{13}CS$ | 231.221 | 53 | $CH_3OH$ | 290.07 | 207 | $H_2{}^{13}CO$ | 343.326 | 32 |
| $H^{13}CN$ | 172.678 | 46 | H$\alpha$ | 231.901 | 80 | $CH_3OH$ | 290.111 | 268 | $HC^{15}N$ | 344.2 | 55 |
| $H^{13}CN$ | 172.678 | 86 | He$\alpha$ | 231.995 | 25 | $CH_3OH$ | 290.185 | 50 | SO | 344.311 | 145 |
| $H^{13}CN$ | 172.68 | 15 | $CH_3OH$ | 234.683 | 19 | $CH_3OH$ | 290.19 | 25 | $CH_3SH$ | 345.021 | 15 |
| $HC_3N$ | 172.849 | 239 | $CO^+$ | 235.79 | 32 | $CH_3OH$ | 290.191 | 25 | $H^{13}CN$ | 345.34 | 298 |
| HCO | 173.377 | 19 | $CO^+$ | 236.063 | 57 | $CH_3OH$ | 290.21 | 15 | CO | 345.796 | 112202 |
| $H^{13}CO^+$ | 173.507 | 194 | $HC_3N$ | 236.513 | 102 | $CH_3OH$ | 290.213 | 27 | NS | 345.823 | 20 |
| SiO | 173.688 | 141 | $H_2CS$ | 236.727 | 50 | $CH_3OH$ | 290.249 | 112 | NS | 345.824 | 15 |
| $HN^{13}C$ | 174.179 | 98 | $HC_3N$,v7=1 | 237.432 | 16 | $CH_3OH$ | 290.264 | 50 | NS | 346.221 | 17 |
| $H_2CS$ | 174.345 | 27 | $NH_2CN$ | 238.316 | 18 | $CH_3OH$ | 290.307 | 81 | SO | 346.528 | 236 |
| $C_2H$ | 174.663 | 658 | $CH_3CN$ | 239.12 | 39 | $CH_3OH$ | 290.308 | 94 | $HC_3N$,v7=1 | 346.949 | 42 |

**Table D.1.** continued.

| Formula | $\nu$ (GHz) | $S$ (mJy) | Formula | $\nu$ (GHz) | $S$ (mJy) | Formula | $\nu$ (GHz) | $S$ (mJy) | Formula | $\nu$ (GHz) | $S$ (mJy) |
|---|---|---|---|---|---|---|---|---|---|---|---|
| $C_2H$ | 174.668 | 446 | $CH_3CN$ | 239.138 | 85 | $CH_3C_2H$ | 290.452 | 54 | $H^{13}CO^+$ | 346.998 | 252 |
| $C_2H$ | 174.722 | 382 | $CH_3C_2H$ | 239.211 | 60 | $CH_3C_2H$ | 290.48 | 63 | SiO | 347.331 | 100 |
| $C_2H$ | 174.728 | 165 | $CH_3C_2H$ | 239.234 | 72 | $CH_3C_2H$ | 290.497 | 106 | $HN^{13}C$ | 348.34 | 130 |
| $C_2H$ | 174.733 | 103 | $CH_3C_2H$ | 239.248 | 121 | $CH_3C_2H$ | 290.502 | 125 | $H_2CS$ | 348.532 | 50 |
| $C_2H$ | 174.807 | 90 | $CH_3C_2H$ | 239.252 | 143 | $H_2CO$ | 290.623 | 449 | $C_2H$ | 349.337 | 934 |
| H$\alpha$ | 174.996 | 63 | $CH_3OH$ | 239.746 | 119 | $HC_3N$ | 291.068 | 22 | $C_2H$ | 349.339 | 751 |
| He$\alpha$ | 175.067 | 20 | H$\beta$ | 240.021 | 43 | $C^{33}S$ | 291.486 | 45 | $C_2H$ | 349.399 | 737 |
| HNCO | 175.189 | 24 | $H_2CS$ | 240.266 | 27 | OCS | 291.84 | 34 | $C_2H$ | 349.4 | 553 |
| HNCO | 175.189 | 18 | HNCO | 240.876 | 29 | $HC_3N$,v7=1 | 292.199 | 29 | $CH_3CN$ | 349.427 | 19 |
| HNCO | 175.189 | 21 | HNCO | 240.876 | 26 | $CH_3OH$ | 292.673 | 144 | $CH_3CN$ | 349.454 | 40 |
| HNCO | 175.844 | 106 | HNCO | 240.876 | 24 | $CH_3OH$ | 293.464 | 35 | $CH_3OH$ | 350.688 | 255 |
| HNCO | 175.844 | 82 | $C^{34}S$ | 241.016 | 233 | CS | 293.912 | 1674 | NO | 350.689 | 373 |
| HNCO | 175.844 | 94 | $NH_2CN$ | 241.479 | 19 | $CH_3CN$ | 294.28 | 32 | NO | 350.691 | 274 |
| HNCO | 176.472 | 21 | $CH_3OH$ | 241.7 | 133 | $CH_3CN$ | 294.302 | 70 | NO | 350.695 | 199 |
| HNCO | 176.472 | 24 | $CH_3OH$ | 241.767 | 175 | SO | 296.55 | 166 | NO | 350.73 | 24 |
| HNCO | 176.472 | 18 | HNCO | 241.774 | 128 | $NH_2CN$ | 297.869 | 20 | NO | 350.737 | 24 |
| HCN | 177.26 | 423 | HNCO | 241.774 | 116 | $^{34}SO$ | 298.258 | 18 | $CH_3OH$ | 350.905 | 728 |
| HCN | 177.26 | 557 | HNCO | 241.774 | 106 | NS | 299.7 | 32 | NO | 350.963 | 24 |
| HCN | 177.261 | 1175 | $CH_3OH$ | 241.791 | 230 | NS | 299.701 | 23 | NO | 350.99 | 24 |
| HCN | 177.261 | 1987 | $CH_3OH$ | 241.833 | 18 | NS | 300.099 | 27 | NO | 351.044 | 374 |
| HCN | 177.262 | 29 | $CH_3OH$ | 241.833 | 18 | $HC_3N$ | 300.16 | 16 | NO | 351.051 | 275 |
| HCN | 177.263 | 423 | $CH_3OH$ | 241.842 | 40 | c-$C_3H_2$ | 300.192 | 52 | NO | 351.052 | 199 |
| H$\beta$ | 177.723 | 33 | $CH_3OH$ | 241.844 | 20 | $H_2S$ | 300.506 | 189 | $SO_2$ | 351.257 | 15 |
| $HCO^+$ | 178.375 | 3369 | $CH_3OH$ | 241.879 | 94 | $H_2CO$ | 300.837 | 567 | c-$C_3H_2$ | 351.523 | 64 |
| SO | 178.605 | 144 | $CH_3OH$ | 241.888 | 40 | SO | 301.286 | 160 | HNCO | 351.633 | 45 |
| $HOC^+$ | 178.972 | 108 | $CH_3OH$ | 241.904 | 66 | $HC_3N$,v7=1 | 301.325 | 31 | HNCO | 351.633 | 43 |
| $C_3H^+$ | 179.903 | 25 | $CH_3OH$ | 241.905 | 76 | $CH_3OH$ | 302.37 | 157 | HNCO | 351.633 | 40 |
| $CH_2NH$ | 180.627 | 39 | HNCO | 242.64 | 29 | $CH_3OH$ | 303.367 | 496 | $H_2CO$ | 351.769 | 426 |
| $CH_3OH$ | 181.296 | 23 | HNCO | 242.64 | 24 | SiO | 303.927 | 154 | c-$C_3H_2$ | 351.782 | 20 |
| HNC | 181.325 | 2064 | HNCO | 242.64 | 26 | OCS | 303.993 | 31 | c-$C_3H_2$ | 351.966 | 56 |
| $CH_3OH$ | 181.771 | 15 | $C^{33}S$ | 242.914 | 47 | SO | 304.078 | 269 | c-$C_3H_2$ | 352.194 | 59 |
| $HC_3N$ | 181.945 | 226 | OCS | 243.218 | 39 | $CH_3OH$ | 304.208 | 635 | H$\alpha$ | 353.623 | 110 |
| OCS | 182.427 | 29 | $CH_3OH$ | 243.916 | 122 | $H_2CS$ | 304.306 | 55 | $CO^+$ | 353.741 | 26 |
| $C_2S$ | 182.553 | 15 | $H_2CS$ | 244.048 | 52 | $C_2H_5OH$ | 305.354 | 15 | He$\alpha$ | 353.767 | 34 |
| $CH_3CN$ | 183.949 | 31 | c-$C_3H_2$ | 244.222 | 39 | $C_2H_5OH$ | 305.434 | 15 | $H_2{}^{13}CO$ | 353.812 | 23 |
| $CH_2NH$ | 183.957 | 20 | CS | 244.936 | 1886 | $CH_3OH$ | 305.473 | 513 | $CO^+$ | 354.014 | 37 |
| $CH_2NH$ | 183.957 | 29 | $CH_2NH$ | 245.126 | 35 | $^{13}CH_3OH$ | 305.699 | 17 | c-$C_3H_2$ | 354.143 | 22 |
| $CH_3CN$ | 183.963 | 67 | $HC_3N$ | 245.606 | 83 | $CH_2NH$ | 306.172 | 31 | HCN,v2 | 354.46 | 149 |
| c-$C_3H_2$ | 184.33 | 61 | $HC_3N$,v7=1 | 246.561 | 18 | $CH_2NH$ | 306.172 | 47 | HCN | 354.505 | 6497 |
| $^{13}CS$ | 184.982 | 54 | $CH_3OH$ | 247.229 | 22 | HNCO | 306.554 | 18 | $CH_3NH_2$ | 354.844 | 24 |
| $N_2H^+$ | 186.345 | 648 | NO | 250.437 | 138 | HNCO | 306.554 | 17 | $HC_3N$,v7=1 | 356.072 | 44 |
| $CH_3C_2H$ | 187.961 | 47 | NO | 250.441 | 87 | HNCO | 306.554 | 16 | HCN,v2 | 356.256 | 151 |
| $CH_3C_2H$ | 187.979 | 56 | NO | 250.449 | 51 | $CH_3OH$ | 307.166 | 453 | $HCO^+$ | 356.734 | 7789 |
| $CH_3C_2H$ | 187.99 | 96 | NO | 250.475 | 16 | $H_3O^+$ | 307.192 | 178 | $HC_3N$,v7=2 | 356.937 | 15 |
| $CH_3C_2H$ | 187.994 | 114 | NO | 250.483 | 16 | H$\beta$ | 307.258 | 52 | $CH_3NH_2$ | 357.44 | 24 |
| $HC_3N$ | 191.04 | 209 | NO | 250.708 | 16 | $^{13}CH_3OH$ | 307.311 | 15 | $C_2H_5OH$ | 357.681 | 16 |
| H$\beta$ | 191.057 | 35 | NO | 250.753 | 16 | $CH_3C_2H$ | 307.53 | 48 | $C_2H_5OH$ | 357.682 | 16 |
| $CH_2NH$ | 191.463 | 39 | NO | 250.796 | 138 | $CH_3C_2H$ | 307.56 | 56 | $HOC^+$ | 357.922 | 248 |
| $CH_2NH$ | 191.463 | 56 | NO | 250.816 | 87 | $CH_3C_2H$ | 307.577 | 94 | $CH_3OH$ | 358.606 | 280 |
| H$\alpha$ | 191.657 | 68 | NO | 250.817 | 52 | $CH_3C_2H$ | 307.583 | 112 | $CH_3C_2H$ | 358.757 | 28 |
| He$\alpha$ | 191.735 | 21 | c-$C_3H_2$ | 251.314 | 193 | HNCO | 307.694 | 82 | $CH_3C_2H$ | 358.791 | 33 |
| $CH_3OH$ | 191.811 | 76 | c-$C_3H_2$ | 251.509 | 53 | HNCO | 307.694 | 76 | $CH_3C_2H$ | 358.811 | 56 |
| $CH_2NH$ | 192.212 | 27 | $CH_3OH$ | 251.738 | 23 | HNCO | 307.694 | 71 | $CH_3C_2H$ | 358.818 | 66 |
| $HOCO^+$ | 192.435 | 24 | $CH_3OH$ | 251.812 | 33 | $CH_3NH_2$ | 307.792 | 32 | $CH_3OH$ | 361.852 | 25 |
| $C^{34}S$ | 192.818 | 178 | SO | 251.826 | 145 | $H_2CS$ | 308.748 | 29 | $NH_2CN$ | 362.143 | 15 |
| $CH_3OH$ | 193.415 | 87 | $CH_3OH$ | 251.867 | 39 | HNCO | 308.798 | 18 | HNC,v2=1 | 362.554 | 45 |
| $CH_3OH$ | 193.442 | 112 | $CH_3OH$ | 251.891 | 33 | HNCO | 308.798 | 17 | HNC | 362.63 | 3526 |
| $CH_3OH$ | 193.454 | 151 | $CH_3OH$ | 251.896 | 23 | HNCO | 308.798 | 16 | $H_2CO$ | 362.736 | 329 |
| $CH_3OH$ | 193.488 | 24 | $CH_3OH$ | 251.9 | 39 | $CH_3OH$ | 309.29 | 346 | $CH_3OH$ | 363.74 | 101 |
| c-$C_3H_2$ | 193.489 | 55 | $CH_3OH$ | 251.906 | 31 | SO | 309.502 | 16 | HNC,v2=1 | 365.147 | 45 |
| $CH_3OH$ | 193.507 | 61 | $CH_3OH$ | 251.917 | 31 | $CH_3OH$ | 310.193 | 213 | $HC_3N$,v7=1 | 365.195 | 46 |
| $CH_3OH$ | 193.511 | 24 | $C_2H_5OH$ | 252.951 | 18 | $HC_3N$,v7=1 | 310.451 | 33 | $HC_3N$,v7=2 | 365.933 | 15 |
| $CH_3OH$ | 193.511 | 38 | $C_2H_5OH$ | 252.952 | 18 | $CH_3NH_2$ | 310.528 | 31 | $HC_3N$,v7=2 | 366.235 | 15 |
| $CH_3OH$ | 193.511 | 44 | NS | 253.57 | 33 | $CH_3OH$ | 311.853 | 233 | $H_2{}^{13}CO$ | 366.27 | 32 |
| $C^{33}S$ | 194.337 | 36 | NS | 253.971 | 33 | $CH_3CN$ | 312.664 | 28 | H$\beta$ | 366.653 | 59 |
| OCS | 194.586 | 32 | $CH_3OH$ | 254.015 | 60 | $CH_3CN$ | 312.688 | 60 | $CH_2NH$ | 367.072 | 28 |
| $CH_3OH$ | 195.147 | 79 | $CH_2NH$ | 254.685 | 63 | $SO_2$ | 313.28 | 21 | $CH_2NH$ | 367.072 | 33 |
| $C_2S$ | 195.375 | 15 | $CH_2NH$ | 254.685 | 83 | $CH_3OH$ | 313.597 | 29 | $CH_3NH_2$ | 367.681 | 17 |
| CS | 195.954 | 1566 | $HC_3N$ | 254.7 | 66 | $H_2CS$ | 313.715 | 56 | $CH_3CN$ | 367.834 | 31 |

**Table D.1.** continued.

| Formula | $\nu$ (GHz) | $S$ (mJy) | Formula | $\nu$ (GHz) | $S$ (mJy) | Formula | $\nu$ (GHz) | $S$ (mJy) | Formula | $\nu$ (GHz) | $S$ (mJy) |
|---|---|---|---|---|---|---|---|---|---|---|---|
| HNCO | 197.085 | 24 | c-$C_3H_2$ | 254.988 | 45 | $^{13}C^{18}O$ | 314.12 | 18 | $H_2S$ | 369.101 | 460 |
| HNCO | 197.085 | 27 | OCS | 255.374 | 38 | $^{13}C^{18}O$ | 314.12 | 25 | $H_2S$ | 369.127 | 32 |
| HNCO | 197.085 | 22 | $HC^{18}O^+$ | 255.48 | 67 | $CH_3OH$ | 314.86 | 139 | $CH_3SH$ | 369.394 | 17 |
| HNCO | 197.821 | 110 | $HC_3N$,v7=1 | 255.689 | 20 | $CH_3OH$ | 315.267 | 119 | $CH_3NH_2$ | 370.166 | 51 |
| HNCO | 197.821 | 123 | $HCS^+$ | 256.028 | 28 | OCS | 316.146 | 28 | $H_2CS$ | 371.844 | 40 |
| HNCO | 197.821 | 98 | $CH_3C_2H$ | 256.293 | 60 | H$\alpha$ | 316.415 | 101 | $N_2H^+$ | 372.673 | 1281 |

by the LTE model should be consistent with the observed spectra and no big outliers should be present. This may not be the case with previously reported species showing some out of equilibrium transitions reported above.

In this section we present details of the modeling of $C_2H_5OH$, HOCN and $HC_3HO$, since most relevant details regarding the newly detected isotopologues are discussed in Sect. 5.4. Figs. D.1, D.2, and D.3 show the fit results to these species where the spectral features are ordered by the brightness of the LTE modeled emission, thus showing only the brightest spectral features of each molecule.

We do not list the spectroscopic parameters of the detected transitions since these are directly extracted from the catalog entries indicated in the figures and more importantly these species have been previously identified in the Galactic ISM.

*$C_2H_5OH$*: All transitions above 3 mJy modeled emission were used to fit the emission of $C_2H_5OH$, where those falling within the spectral features of significantly brighter transitions were masked, adding up to a total of ∼50 transitions considered. Among its brightest transitions only the transitions at 287.944 GHz ($6_{4,2} - 5_{3,3}$) and 287.917 GHz ($6_{4,3} - 5_{3,2}$) form an clearly unblended spectral feature. Other spectral lines at 252.952, 270.450, and 234.758 GHz, though partially blended, confirm the detection of $C_2H_5OH$, together with the fainter feature at 243.556 GHz also marginally blended as displayed in Fig. D.1. The identified transitions appear to show a double peak, similar to what is observed for $CH_3OH$, further supporting this detection.

*HOCN*: The brightest expected transition of HOCN in the whole frequency coverage of ALCHEMIS ($10_{0,10} - 9_{0,9}$ at 209.732 GHz) is unambiguously detected and just marginally blended. The brightness of all other transitions drop quickly below the detection limit or are blended to other brighter species as shown in Fig. D.2. All spectral features shown in this figure, but for the one at 251.666 GHz were used in the fit.

*$HC_3HO$*: The two brighest transitions of $HC_3HO$ ($14_{0,14} - 13_{0,13}$ @ 129.975 GHz and $15_{0,15} - 14_{0,14}$ @ 139.169 GHz) appear unblended in our survey while most other transitions fall close to the noise level of our obsrevations. We conservatively included transitions down to ∼1 mJy in the fit to this species which may have resulted in an understimate of the brightest transitions. A fit performed exclusively with the two brightest transitions would have resulted into a column density 80% higher yielding $N_{HC_3HO} = 10^{14.2} \pm 10^{13.6}$ cm$^{-2}$.

## Appendix E: Extragalactic molecular census

**Table E.1.** Chronology of extragalactic detections.

| Year | Molecule | Reference | Year | Molecule | Reference | Year | Molecule | Reference |
|---|---|---|---|---|---|---|---|---|
| 1971 | OH | 1 | 2003 | $SO_2$ | 38 | 2013 | $C_2$ | 59 |
| 1974 | $H_2CO$ | 2 | 2003 | NO | 38 | 2013 | $C_3$ | 59 |
| 1975 | CO | 3 | 2003 | NS | 38 | 2013 | $HCS^+$ | 60 |
| 1975 | $^{13}CO$ | 4 | 2003 | $^{34}SO$ | 38 | 2013 | $NH_2CHO$ | 60 |
| 1977 | $H_2O$ | 5 | 2004 | $HOC^+$ | 39 | 2013 | $^{30}SiO$ | 60 |
| 1977 | HCN | 6 | 2004 | NH | 40 | 2014 | $H_2Cl^+$ | 61 |
| 1978 | $H_2$ | 7 | 2004 | $OH^+$ | 41,42 | 2014 | $H_2^{37}Cl^+$ | 61 |
| 1979 | $NH_3$ | 8 | 2006 | $C_2S$ | 43 | 2014 | $NH_2$ | 62 |
| 1979 | $HCO^+$ | 9 | 2006 | $NH_2CN$ | 44 | 2014 | $H_2^{17}O$ | 62 |
| 1980 | CH | 10 | 2006 | $HOCO^+$ | 44 | 2014 | $^{13}CN$ | 63 |
| 1985 | CS | 11 | 2006 | c-$C_3H$ | 44 | 2015 | $ArH^+$ | 64 |
| 1986 | c-$C_3H_2$ | 12 | 2006 | DNC † | 44 | 2015 | $^{38}ArH^+$ | 64 |
| 1987 | $CH^+$ | 13,14 | 2006 | $N_2D^+$ † | 44 | 2015 | $HC_5N$ | 65,66,75 |
| 1987 | $CH_3OH$ | 15 | 2006 | $CH_2NH$ | 44,45 | 2015 | $CH_3SH$ | 67,68 |
| 1988 | CN | 16 | 2006 | $HC^{18}O^+$ | 44,46 | 2016 | $CF^+$ | 69 |
| 1988 | $C_2H$ | 16 | 2006 | $HC^{17}O^+$ | 46 | 2017 | $^{13}CH^+$ | 70 |
| 1988 | HNC | 16 | 2006 | $H^{15}NC$ | 46,75 | 2017 | $SH^+$ | 70 |
| 1988 | $HC_3N$ | 16,17 | 2006 | $H_2^{34}S$ | 46 | 2017 | $^{34}SH^+$ | 70 |
| 1989 | HNCO | 18,19 | 2006 | $H_3^+$ | 47 | 2018 | $CH_3OCH_3$ | 71 |
| 1989 | $C^{34}S$ | 20 | 2006 | $C_4H_2$ | 48 | 2018 | $CH_3OCHO$ | 71 |
| 1991 | $C^{18}O$ | 21 | 2006 | $C_6H_2$ | 48 | 2019 | HCl | 72 |
| 1991 | $C^{17}O$ | 21 | 2006 | $C_6H_6$ | 48 | 2019 | HCl | 72 |
| 1991 | SO | 22,23 | 2008 | $H_3O^+$ | 49 | 2020 | $O_2$ † | 73 |
| 1991 | $N_2H^+$ | 24 | 2009 | $C^{33}S$ | 50 | 2020 | l-$C_3H^+$ | 68 |
| 1991 | SiO | 24 | 2009 | $^{13}CH_3OH$ | 51,52,75 | 2020 | $C_3N$ | 68 |
| 1991 | $H^{13}CO^+$ | 24 | 2010 | HF | 53 | 2020 | $CH_2CHCN$ | 68 |
| 1991 | $HN^{13}C$ | 24 | 2010 | $H_2O^+$ | 53,54 | 2020 | $H_2CN$ | 68 |
| 1991 | $H^{13}CN$ | 24 | 2010 | $^{13}C^{18}O$ | 55,56 | 2020 | HCOOH | 68,75 |
| 1991 | $CH_3CCH$ | 25 | 2010 | $C_{60}$ † | 57 | 2020 | ND | 74 |
| 1991 | $CH_3CN$ | 25 | 2011 | $H^{13}CCCN$ | 58 | 2020 | $NH_2D$ | 74 |
| 1993 | $^{13}CS$ | 26 | 2011 | $HC^{13}CCN$ | 58 | 2020 | HDO | 74 |
| 1995 | OCS | 27 | 2011 | $HCC^{13}CN$ | 58 | 2021 | $H_2^{13}CO$ | 75 |
| 1995 | HCO | 28 | 2011 | $H_2^{18}O$ | 58 | 2021 | $C_2H_5OH$ | 75 |
| 1996 | $DCO^+$ | 29 | 2011 | $^{29}SiO$ | 58 | 2021 | $^{13}CCH$ | 75 |
| 1996 | DCN | 29 | 2011 | $CH_2CO$ | 58,45 | 2021 | $C^{13}CH$ | 75 |
| 1998 | LiH † | 30,31 | 2011 | $SO^+$ | 45 | 2021 | HOCN | 75 |
| 1999 | $HC^{15}N$ | 32 | 2011 | l-$C_3H$ | 45 | 2021 | $CH_3^{13}CCH$ | 75 |
| 1999 | $H_2S$ | 33 | 2011 | l-$C_3H_2$ | 45 | 2021 | $CH_3C^{13}CH$ | 75 |
| 1999 | $H_2CS$ | 33,34 | 2011 | $CH_2CN$ | 45 | 2021 | $^{13}CH_3CCH$ | 75 |
| 1999 | $C_2H_2$ | 35 | 2011 | $C_4H$ | 45 | 2021 | $HC_3HO$ | 75 |
| 2000 | $CO^+$ | 36 | 2011 | $CH_3NH_2$ | 45 | 2021 | $Si^{17}O$ † | 75 |
| 2001 | HD | 37 | 2011 | $CH_3CHO$ | 45 | | | |

**Notes.** Year of first detection of each indiviudal molecular species, were first detections of isotopologues are also included. When first detection was tentative, confirmation is also included. (†) Species where only tentative detection have been reported.

**References.** (1) Weliachew (1971); (2) Gardner & Whiteoak (1974); (3) Rickard et al. (1975); (4) Solomon & de Zafra (1975); (5) Churchwell et al. (1977); (6) Rickard et al. (1977); (7) Thompson et al. (1978); (8) Martin & Ho (1979); (9) Stark & Wolff (1979); (10) Whiteoak et al. (1980); (11) Henkel & Bally (1985); (12) Seaquist & Bell (1986); (13) Magain & Gillet (1987); (14) Falgarone et al. (2017); (15) Henkel et al. (1987); (16) Henkel et al. (1988); (17) Mauersberger et al. (1990); (18) Nguyen-Q-Rieu et al. (1989); (19) Nguyen-Q-Rieu et al. (1991); (20) Mauersberger & Henkel (1989); (21) Sage et al. (1991); (22) Johansson (1991); (23) Petuchowski & Bennett (1992); (24) Mauersberger & Henkel (1991); (25) Mauersberger et al. (1991); (26) Henkel et al. (1993); (27) Mauersberger et al. (1995); (28) Sage & Ziurys (1995); (29) Chin et al. (1996); (30) Combes & Wiklind (1998); (31) Friedel et al. (2011); (32) Chin et al. (1999); (33) Heikkilä et al. (1999); (34) Martín et al. (2005); (35) van Loon et al. (1999); (36) Fuente et al. (2000); (37) Varshalovich et al. (2001); (38) Martín et al. (2003); (39) Usero et al. (2004); (40) González-Alfonso et al. (2004); (41) González-Alfonso et al. (2004); (42) van der Werf et al. (2010); (43) Martín et al. (2006); (44) Martín et al. (2006); (45) Muller et al. (2011); (46) Muller et al. (2006); (47) Geballe et al. (2006); (48) Bernard-Salas et al. (2006); (49) van der Tak et al. (2008); (50) Wang et al. (2009); (51) Martín et al. (2009a); (52) Muller et al. (2021); (53) van der Werf et al. (2010); (54) Weiß et al. (2010); (55) Martín et al. (2010); (56) Martín et al. (2019b); (57) García-Hernández et al. (2010); (58) Martín et al. (2011); (59) Welty et al. (2013); (60) Muller et al. (2013); (61) Muller et al. (2014a); (62) Muller et al. (2014b); (63) Takano et al. (2014); (64) Müller et al. (2015); (65) Aladro et al. (2015); (66) Costagliola et al. (2015); (67) Meier et al. (2015); (68) Tercero et al. (2020); (69) Muller et al. (2016); (70) Muller et al. (2017); (71) Sewiło et al. (2018); (72) Wallström et al. (2019); (73) Wang et al. (2020); (74) Muller et al. (2020); (75) This work.

The continuous growth of new species detected during the last two decades has resulted in various publications reporting up to date listings of the extragalactic molecular census including conference proceedings (Martín 2009; Martín et al. 2011), refereed publications (Martín et al. 2006, 2011; McGuire 2018), as well as online resources such as that hosted at CDMS[6]. Each of these reports have had different formats and criteria depending on the scope of the publication but all aiming to maintain updated information on first molecular extragalactic detections. Despite these available resources, given the legacy value of ALCHEMI for the extragalactic molecular content, and the relevance of isotopologue detections in this work, which are not included in most of the references above, we provide here a detailed and updated extragalactic molecular census.

In this appendix we provide a comprehensive listing of all molecular species and isotopologues detected in the extragalactic ISM according to the chronology of detections (Table E.1) and grouped by the number of atoms in the molecule (Table E.2). Graphical representations of these lists can be found in Sect. 4.4.

**Table E.2.** Census of extragalactic molecular species and isotopologues detected.

| 2 atoms | 3 atoms | 4 atoms | 5 atoms | 6 atoms | 7 atoms | > 7 atoms |
|---|---|---|---|---|---|---|
| $ArH^+$, $^{38}ArH^+$ | $C_2H$, $^{13}CCH$, $C^{13}CH$ | $C_2H_2$ | $C_4H$ | $C_4H_2$ | $CH_2CHCN$ | $C_2H_5OH$ |
| $C_2$ | $C_2S$ | $C_3N$ | c-$C_3H_2$ | $CH_3CN$ | $CH_3CCH$, $^{13}CH_3CCH$, $CH_3^{13}CCH$, $CH_3C^{13}CH$ | $C_6H_2$ |
| $CF^+$ | $C_3$ | c-$C_3H$ | l-$C_3H_2$ | $CH_3OH$, $^{13}CH_3OH$ | $CH_3CHO$ | $C_6H_6$ |
| CH | $H_2Cl^+$, $H_2^{37}Cl^+$ | l-$C_3H$ | $CH_2CN$ | $CH_3SH$ | $CH_3NH_2$ | $C_{60}$ † |
| $CH^+$, $^{13}CH^+$ | $H_2O$, $H_2^{18}O$, $H_2^{17}O$, HDO | l-$C_3H^+$ | $CH_2CO$ | $HC_3HO$ | $HC_5N$ | $CH_3OCH_3$ |
| CN, $^{13}CN$ | $H_2O^+$ | $H_2CN$ | $CH_2NH$ | $NH_2CHO$ | | |
| CO, $^{13}CO$, $C^{18}O$, $C^{17}O$, $^{13}C^{18}O$ | $H_2S$, $H_2^{34}S$ | $H_2CO$, $H_2^{13}CO$ | $HC_3N$, $H^{13}CCCN$, $HC^{13}CCN$, $HCC^{13}CN$ | | | $CH_3OCHO$ |
| $CO^+$ | $H_3^+$ | $H_2CS$ | HCOOH | | | |
| CS, $^{13}CS$, $C^{34}S$, $C^{33}S$ | HCN, $H^{13}CN$, $HC^{15}N$, DCN † | $H_3O^+$ | $NH_2CN$ | | | |
| $H_2$, HD | HCO | HNCO | | | | |
| HF | $HCO^+$, $H^{13}CO^+$, $HC^{18}O^+$, $HC^{17}O^+$, $DCO^+$ | HOCN | | | | |
| LiH † | $HCS^+$ | $HOCO^+$ | | | | |
| NH, ND | HNC, $HN^{13}C$, $H^{15}NC$, DNC | $NH_3$, $NH_2D$ | | | | |
| NO | $HOC^+$ | | | | | |
| NS | $N_2H^+$, $N_2D^+$ † | | | | | |
| $O_2$ † | $NH_2$ | | | | | |
| OH | OCS | | | | | |
| $OH^+$ | $SH^+$, $^{34}SH^+$ | | | | | |
| SiO, $^{29}SiO$, $^{30}SiO$, $Si^{17}O$ † | $SO_2$ | | | | | |
| SO, $^{34}SO$ | | | | | | |
| $SO^+$ | | | | | | |

**Notes.** Species are alphabetically ordered in each column. (†) Sppecies where only tentative detections have been reported. The table is updated from Martín et al. (2011) according to the list of detections in Table E.1, were references for each detection are provided.

[6] https://cdms.astro.uni-koeln.de/classic/molecules

## Appendix F: Full spectrum and model

Fig. F.1 presents the full spectrum analyzed in this article (gray histogram) with the best LTE model fit (red line) as well as the labels for each individual transition with flux density above 100 mJy according to the LTE model. Figs. F.2 to F.11 present a zoomed version of Fig. F.1 in 5 GHz windows and labeling transitions down to 2 mJy. We note that despite what was indicated in Table A.1, the spectral window centered at 368.7 GHz could not be imaged with the 12 m data due to the poor atmospheric transmission. Despite the poorer quality of the data, this spectral window is included in Fig. F.11, which actually shows a bright spectral feature due to $H_2S$. The quality of the data can only be used to confirm the presence of the line but was not included in the fit.

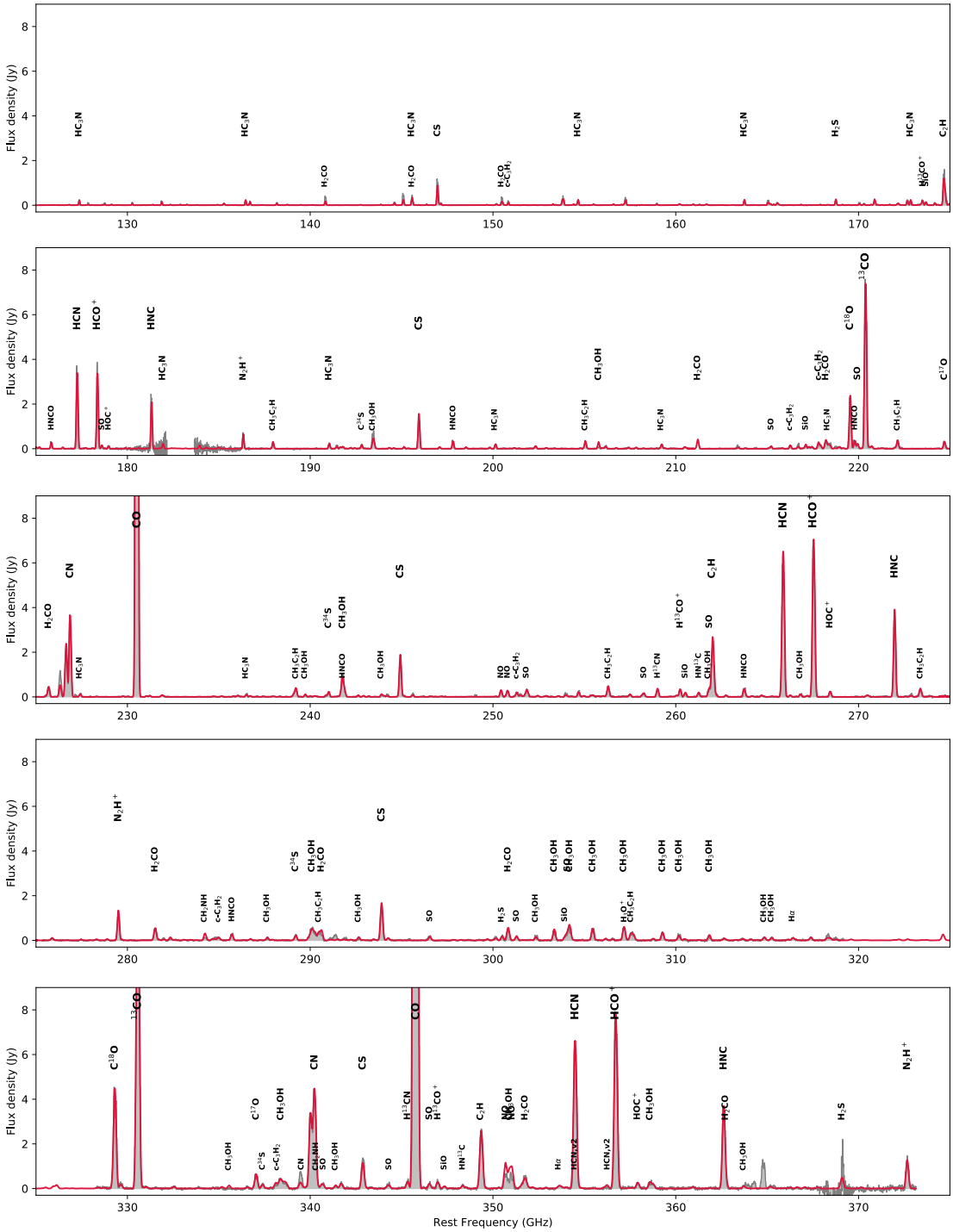


**Fig. F.1.** Full spectral coverage as in Fig.4 zoomed to 50 GHz frequency windows. The observed spectrum is shown in grey histogram and the model (Sect. 4.3.2) in red line. Only the brighter individual molecular transitions with intensities higher than 100 mJy are labeled with different y-axis position and character size depending on the modelled intensity for > 5, > 1,> 0.2, and > 0.1 Jy.

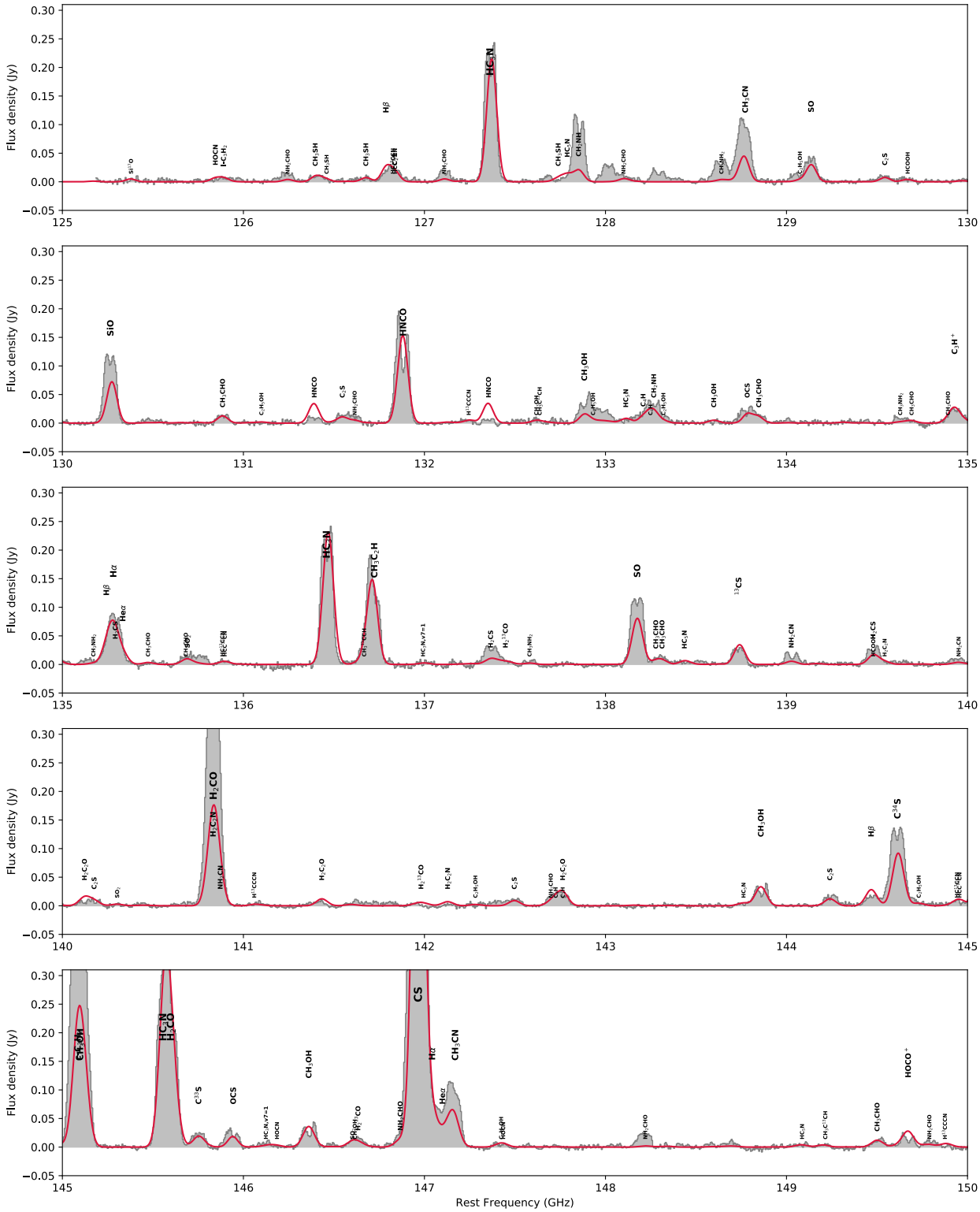


**Fig. F.2.** Full spectral coverage as in Fig.4 zoomed to 5 GHz frequency windows. The observed spectrum is shown in grey histogram and the model (Sect. 4.3.2) in red line. Individual molecular transitions with intensities higher than 2 mJy are labeled with different y-axis position and character size depending on the modelled intensity for > 270, > 95, > 40, > 20, > 15, > 10, > 5, and > 2 mJy.

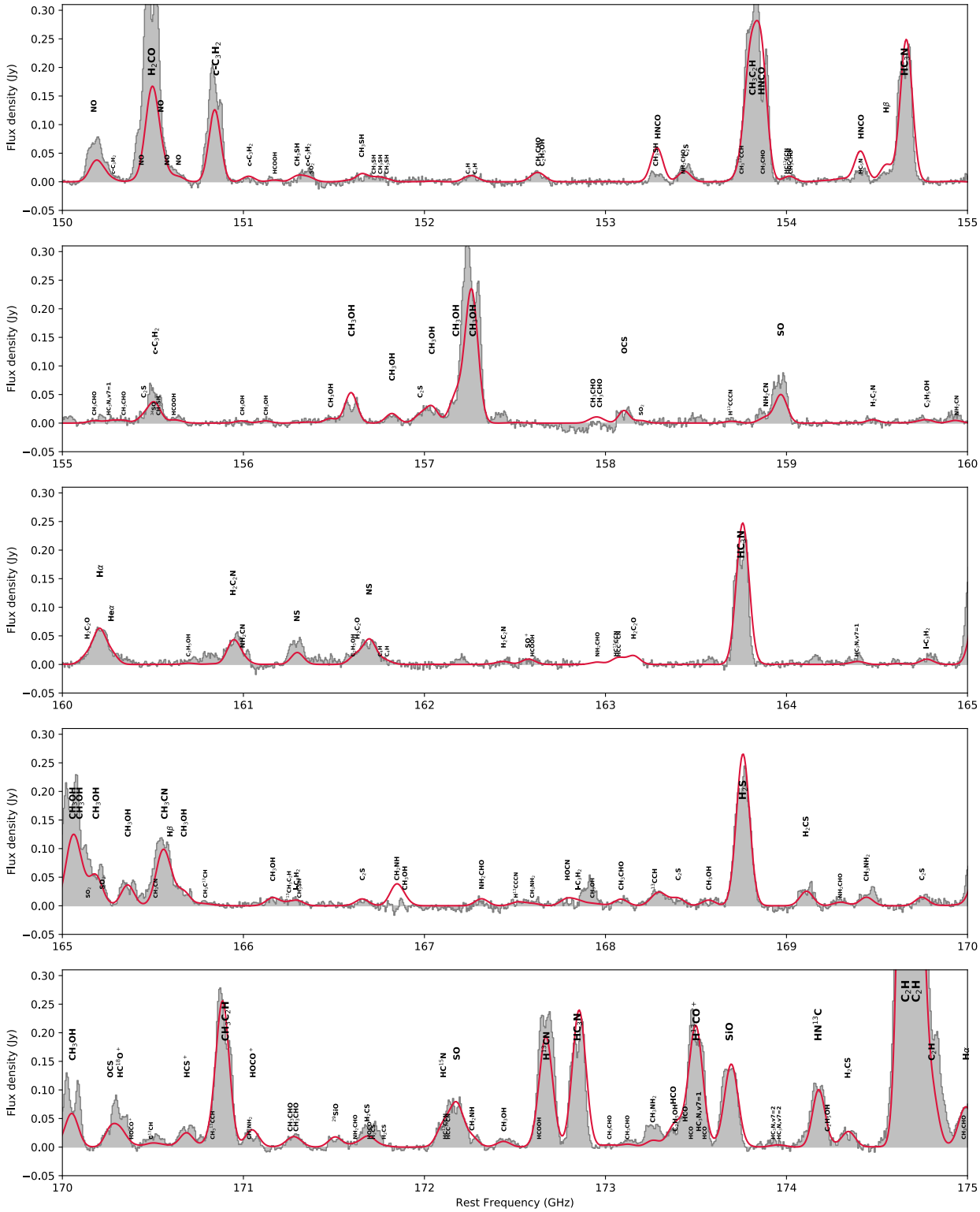


**Fig. F.3.** Same as Fig. F.2.

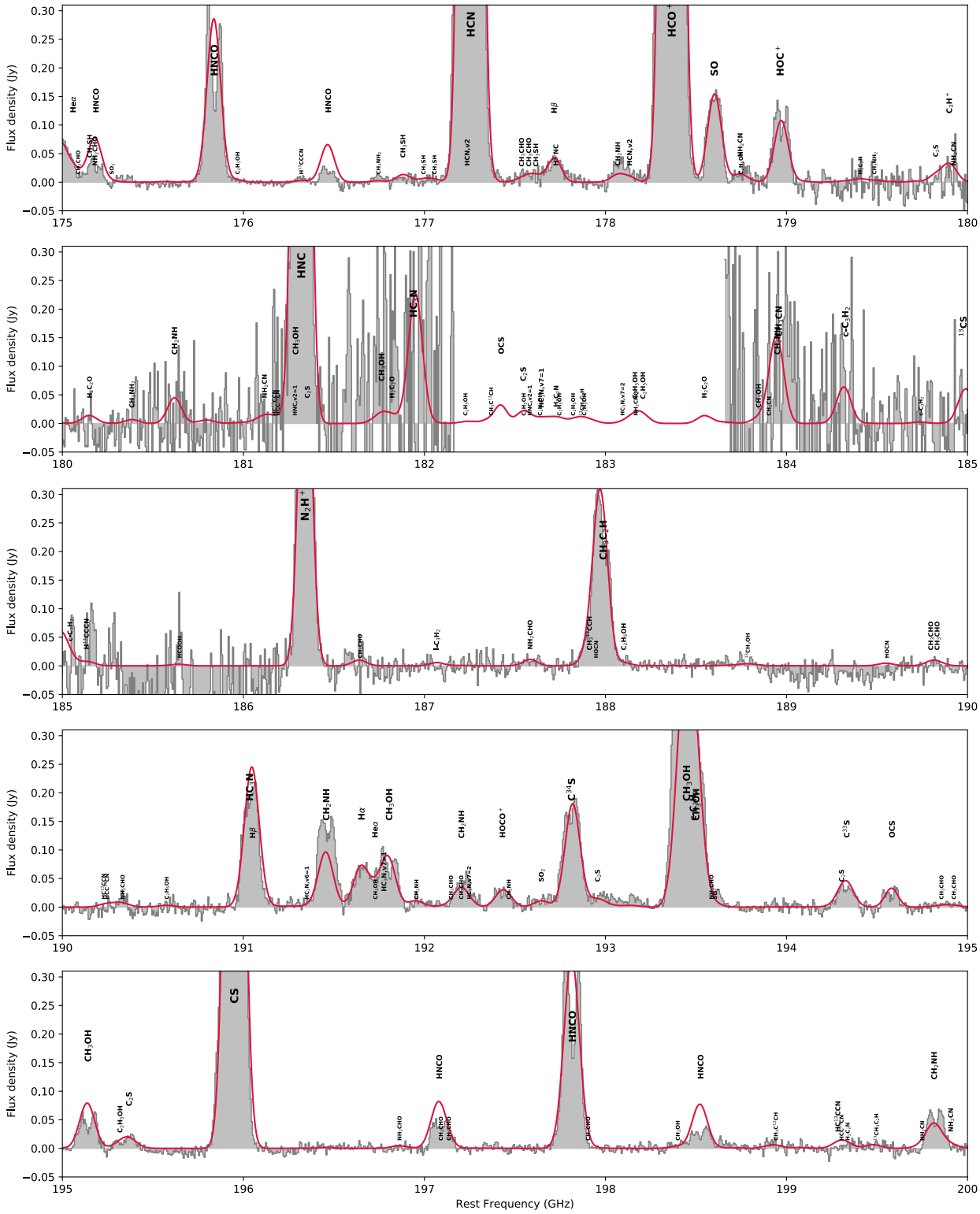


**Fig. F.4.** Same as Fig. F.2.